Size-Dependent Oscillatory Magnetoresistance Effect in Gallium*†

J. A. MUNARIN‡ AND J. A. MARCUS
Northwestern University, Evanston, Illinois 60201

AND

PHILIP E. BLOOMFIELD
University of Pennsylvania, Philadelphia, Pennsylvania 19104

(Received 8 February 1968)

The nonmonotonic part of the magnetoresistance has been measured in five single crystals of gallium at 1.2°K in the range 0 to 16 kOe using the audio-frequency field-modulation technique. The transverse coefficients were found to oscillate directly with the magnetic field with nondecreasing amplitude in the high-field region defined by $\omega_c\tau \gg 1$. A large number of periods have been resolved by Fourier analysis of the data in the *ab* and *ac* planes, and a study has been made of the orientation and size dependence of the oscillation frequencies. Formulas are presented for the oscillatory frequencies and amplitudes giving their dependence on magnetic field strength and orientation, Fermi-surface parameters, and sample size. Theory suggests that the high-field amplitude growth may be correlated with the form of the conductivity tensor for a compensated metal and the diffusivity of the sample surface seen by electrons having extremal values of $m^*\langle v_z\rangle$. Nearly-free-electron-model calculations show that electrons from the seventh and eighth band surfaces in gallium have these properties. Evidence for magnetic breakdown across the (100) face of the Brillouin zone is presented.

I. INTRODUCTION

OSCILLATIONS in the galvanomagnetic coefficients of thin metallic samples of the type predicted by Sondheimer[1] were discovered by Babiskin and Siebenmann[2] in polycrystalline sodium wires and in thin films by Cotti.[3] More recently, Forsvoll and Holwech[4] found pronounced oscillations in polycrystalline aluminum films, and similar effects were studied in single crystals of cadmium by Zebouni, Hamburg, and Mackey.[5] These periodic fluctuations in the magnetoresistivity are not related to the de Haas–Schubinkov effect, but are associated with conduction electrons at the elliptical limiting points[6] on the Fermi surface (FS) which are resonantly scattered from the plane-parallel surface boundaries of the specimen. At low temperatures where the electronic mean free path is large compared to the sample thickness d, collisions within the bulk are relatively rare, and the conductivity becomes modified with respect to its monotonic value according to the deviations from the condition

$$\omega_c d = 2\pi n \cos\theta \langle v_z\rangle, \tag{1}$$

which matches the transit time for electrons drifting across the sample to the cyclotron period $2\pi/\omega_c$. Here, θ is the angle which the field makes with the sample surface perpendicular, and $\langle v_z\rangle$ is equal to the projection of the electron velocity along H averaged over the orbit. From Eq. (1) the boundary-scattering term in the conductivity oscillates *directly* in H with period given by

$$\Delta H = 2\pi m^* c\langle v_z\rangle (ed\sec\theta)^{-1}, \tag{2}$$

where m^* is the cyclotron effective mass.

The Sondheimer oscillations in the conductivity are essentially a low-field effect with amplitude proportional to H^{-4} in the high-field region $\omega_c\tau \gg 1$, where τ is the bulk scattering time.[7,8] Gurevich[7] found that similar effects with different amplitude dependences may be present when the FS is more complicated, and it was pointed out by Grenier, Efferson, and Reynolds[8] that "magnetomorphic" effects should occur more generally whenever the derivative $(\partial A/\partial k_z)_{\epsilon_F}$ has an extremum or a singularity, which is the case for limiting points, inflection zones, and truncated and "monochromatic" (parabolic) energy surfaces. The latter type gives rise to oscillations in the conductivity which fall off as H^{-2} at high fields while the size-dependent component in the magnetoresistivity approaches a constant amplitude, as was pointed out independently by one of the present authors[9] (see Sec. II).

We have found a complex low-amplitude size-dependent component of magnetoresistance periodic in H in single crystals of high-purity gallium[10] at liquid-

* Supported by the Advanced Research Projects Agency and the National Science Foundation.

† Part of this work is based on a dissertation submitted to the graduate school of Northwestern University by J. A. Munarin in partial fulfillment of the requirements for the degree of Doctor of Philosophy.

‡ Present address: Department of Physics, Indiana University, Bloomington, Ind.

[1] E. H. Sondheimer, Nature **164**, 920 (1949); see also Phys. Rev. **80**, 401 (1950).

[2] Julius Babiskin and P. G. Siebenmann, Phys. Rev. **107**, 1249 (1957).

[3] P. Cotti, in *High Magnetic Fields*, edited by H. Kolm, B. Lax, F. Bitter, and R. Mills (Tech Press, Cambridge, 1962).

[4] K. Forsvoll and I. Holwech, Phil. Mag. **9**, 435 (1964).

[5] N. H. Zebouni, R. E. Hamburg, and H. J. Mackey, Phys. Rev. Letters **11**, 260 (1963).

[6] The limiting points of the Fermi surface are defined as the points of contact with tangent planes perpendicular to the magnetic field direction.

[7] V. L. Gurevich, Zh. Eksperim. i Teor. Fiz. **35**, 668 (1958) [English transl.: Soviet Phys.—JETP **8**, 464 (1959)].

[8] C. G. Grenier, K. R. Efferson, and J. M. Reynolds, Phys. Rev. **143**, 406 (1966).

[9] P. Bloomfield, Bull. Am. Phys. Soc. **11**, 170 (1966).

[10] J. A. Munarin and J. A. Marcus, in *Proceedings of the Ninth International Conference on Low-Temperature Physics* (Plenum Press, Inc., New York, 1965), p. 743; Bull. Am. Phys. Soc. **10**, 351 (1965); **11**, 170 (1966).

helium temperatures and have studied the effect as a function of both field orientation and sample geometry. Oscillations in the transverse components investigated primarily in the range 0 to 16 kOe exhibit anomalous growth of amplitude with magnetic field and are undiminished in size to at least 30 kOe.[11] The complicated frequency spectrum has been determined for five samples with H in the ab and ac planes (Sec. IV); these measurements are interpreted on the basis of the nearly-free-electron (NFE) model in Sec. V. It is shown that many of the effective orbits have the function $(\partial^2 A/\partial k_z^2)_{\epsilon_F}=0$. The calculations of Sec. II for pure diffuse scattering of the electrons at the sample surface predict that the amplitude of these oscillations will either diminish as $H^{-1/2}$ or become constant in high fields when either open orbits are excited or the metal is uncompensated; however, for a compensated metal the calculations indicate their amplitude will grow more rapidly than H. In Sec. V the experimental behavior of the resistivity and Hall effect as a function of magnetic field orientation and strength are accounted for in terms of the angular dependence of the effective sample area, the transit distance, and the magnitude of the "acceleration" of the frequency of oscillation, and by the fact that the effective diffusivity depends on the orbit size and that near the surface there is additional scattering of the oscillating electrons by open-orbit current sheets.

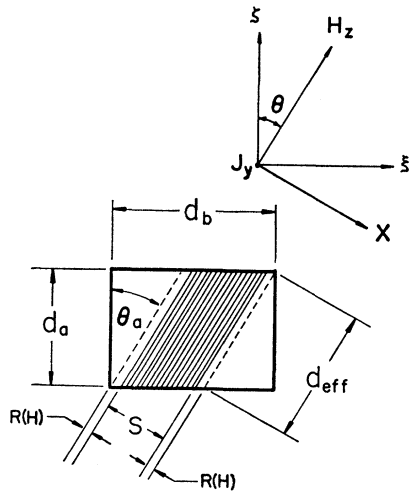

FIG. 1. Top: comparison of crystalline- and magnetic field–coordinate system. Bottom: $R(H)$ is the cyclotron radius and d_{eff} is equal to $d_a \sec\theta_a$. We neglect the corrections due to finite size of orbit on the effective area contributing to the oscillatory resistivity [$R(H)\ll S$ for $H>500$ Oe except when H points along body diagonal]. Sample cross sections showing the effective region contributing to the oscillations for a particular field orientation.

II. THEORY OF THE OSCILLATIONS

In this section we derive expressions for the conductivity tensor assuming no spatial dependence of the electric field and pure diffuse scattering of the electrons at the metal-vacuum interface. In Sec. V a qualitative discussion indicates the modifications due to open-orbit contributions to the static skin effect and the fact that the surface diffusivity can depend on the strength of the magnetic field.

Here we take the magnetic field $H=H_z$ to be strong enough so that the cyclotron diameter is much smaller than the sample dimensions and the electrons communicate between sample surfaces predominantly because of their drift motion. Azbel[12] has shown that for processes where the mean free path is longer than sample dimensions and where there is electron drift across the sample, it is correct to neglect the static skin effect (spatial dependence of E). With τ representing the bulk scattering time and the cyclotron frequency given by

$$\omega_c = eH/m^*c, \tag{3}$$

where e is the magnitude of the electron charge and the orbital or effective mass is given by

$$m^* = \frac{1}{2\pi}\oint \frac{dp}{v_\perp(k_z)}, \tag{4}$$

we have an expression[12–15] for the low-temperature electronic current at the depth ζ in the metal. Here, i,k correspond to the coordinates attached to the magnetic field x, y, z; y is along the current direction (a or c axis), and ζ is the axis connecting the parallel faces pierced by H_z (see Fig. 1, top).

$$J_i(\zeta) = \frac{e^2}{\pi h^2}\int dk_z \frac{m^*}{\omega_c}\oint d\psi\, v_i(\psi,k_z) \times \int_{\varphi(\zeta,\psi,k_z)}^{\psi} d\psi' \exp[(\psi'-\psi)/\omega_c\tau]\sum_k v_k(\psi',k_z)E_k. \tag{5}$$

Since we are considering diffuse scattering, $\varphi(\zeta,\psi,k_z)$ represents the most recent past value of the orbital parameter ψ' such that the electron at (ψ,k_z) is at the depth ζ having started from the sample surface at (φ,k_z).[12,14] The specific value is given by

$$\omega_c^{-1}\int_{\varphi(\zeta,\psi,k_z)}^{\psi} d\psi' v_\zeta(\psi',k_z) = \begin{cases} \zeta, & v_\zeta^0>0 \\ \zeta-d, & v_\zeta^0<0 \end{cases} \tag{6}$$

[11] The corresponding oscillations in the rf differential absorption had been observed by Foner and McNiff in fields up to 43 kOe [see S. Foner and E. J. McNiff, Jr., Bull. Am. Phys. Soc. **10**, 351 (1965)], and more recently they have observed both the dc and rf oscillations (with amplitude much reduced) in fields up to 95 kOe [Rev. Sci. Instr. **38**, 931 (1967)]. In their experiments the rf skin depth is larger than the sample thickness.

[12] M. Ya Azbel, Zh. Eksperim. i Teor. Fiz. **44**, 983 (1963) [English transl.: Soviet Phys.—JETP **17**, 667 (1963)].

[13] E. A. Kaner, Zh. Eksperim. i Teor. Fiz. **34**, 658 (1959) [English transl.; Soviet Phys.—JETP **7**, 454 (1958)].

[14] P. Bloomfield, Physica **32**, 1189 (1966).

[15] R. G. Chambers, Proc. Roy. Soc. (London) **A65**, 458 (1952).

where $0<\zeta<d$, and

$$v_\zeta{}^0=\langle v_\zeta\rangle=\frac{1}{2\pi}\oint d\psi' v_\zeta(\psi',k_z)$$

is the ζ component of the electron drift velocity. The averaged total current across the sample,[16]

$$\frac{1}{d}\int_0^d J_i(\zeta)d\zeta=I_i=\sum_j \sigma_{ij}E_j, \tag{7}$$

is calculated by making a partial integration with respect to ζ and utilization of Eq. (6). This yields an expression for the conductivity tensor in Eq. (7).

$$\begin{aligned}\sigma_{ik}=&\frac{e^2}{\pi h^2}\int_{v_\zeta{}^0>0} dk_z\frac{m^*}{\omega_c}\oint d\psi v_i(\psi,k_z)\left\{\int_{\varphi(d,\psi,k_z)}^{\psi} d\psi' \exp[(\psi'-\psi)/\omega_c\tau]v_k(\psi',k_z)\right.\\ &\left.-(d\omega_c)^{-1}\int_{\varphi(d,\psi,k_z)}^{\varphi(0,\psi,k_z)} d\psi' \exp[(\psi'-\psi)/\omega_c\tau]v_k(\psi',k_z)\int_{\psi'}^{\psi} d\psi'' v_\zeta(\psi'',k_z)\right\}\\ &+\frac{e^2}{\pi h^3}\int_{v_\zeta{}^0<0} dk_z\frac{m^*}{\omega_c}\oint d\psi v_i(\psi,k_z)\left\{\int_{\varphi(0,\psi,k_z)}^{\psi} d\psi' \exp[(\psi'-\psi)/\omega_c\tau]v_k(\psi',k_z)\right.\\ &\left.-(d\omega_c)^{-1}\int_{\varphi(0,\psi,k_z)}^{\varphi(d,\psi,k_z)} d\psi' \exp[(\psi'-\psi)/\omega_c\tau]v_k(\psi',k_z)\left[\omega_c+\int_{\psi'}^{\psi} d\psi'' v_\zeta(\psi'',k_z)\right]\right\}. \end{aligned}\tag{8}$$

Here we have neglected the discontinuous behavior[12,14] of $\varphi(\zeta,\psi,k_z)$ due to the orbital locations, where $v_\zeta=0$. Then by using the identities following from Eq. (6),

$$\begin{aligned}\varphi(d,\psi,v_\zeta{}^0<0)&=\varphi(0,\psi,v_\zeta{}^0>0)=\psi,\\ \varphi(d,\psi,v_\zeta>0)&=\varphi(0,\psi,v_\zeta<0),\end{aligned}\tag{9}$$

and the central symmetry of the FS, $\epsilon(\mathbf{k})=\epsilon(-\mathbf{k})$, we can rewrite Eq. (8) and sum only over those orbits for which $v_\zeta{}^0>0$; i.e., the contributions from all orbits with $v_\zeta{}^0<0$ exactly equals those from $v_\zeta{}^0>0$:

$$\begin{aligned}\sigma_{ik}=&\frac{2e^2}{\pi h^2}\int_{v_\zeta{}^0>0} dk_z\frac{m^*}{\omega_c}\oint d\psi v_i(\psi,k_z)\\ &\times\int_{\varphi(d,\psi,k_z)}^{\psi} d\psi' \exp[(\psi'-\psi)/\omega_c\tau]v_k(\psi',k_z)\\ &\times\left[1-(d\omega_c)^{-1}\int_{\psi'}^{\psi} d\psi'' v_\zeta(\psi'',k_z)\right].\end{aligned}\tag{10}$$

We now represent the velocities in a Fourier series[17,18]:

$$\begin{aligned}v_i(\psi,k_z)&=\sum_{n=0}^{\infty}[v_i{}^{1n}(k_z)\cos n\psi+v_i{}^{2n}(k_z)\sin n\psi]\\ &=\sum_{n=-\infty}^{\infty} v_i{}^{(n)}(k_z)e^{in\psi}\\ &=\sum_{n=0}^{\infty} v_i{}^n(k_z)\cos(n\psi-\psi_i{}^n).\end{aligned}\tag{11}$$

Here,

$$\begin{aligned}v_i{}^{(n)}&=\tfrac{1}{2}[v_i{}^{1n}-i\,\mathrm{sgn}(n)v_i{}^{2n}],\\ v_i{}^n&=[(v_i{}^{1n})^2+(v_i{}^{2n})^2]^{1/2}=2|v_i{}^{(n)}|\\ &=2[v_i{}^{(n)}v_i{}^{(-n)}]^{1/2},\\ \psi_i{}^n&=\arctan(v_i{}^{2n}/v_i{}^{1n}).\end{aligned}\tag{12}$$

Since we are concerned with large magnetic fields, the cyclotron diameter is assumed to be much smaller than the sample thickness and the orbital parameter is approximately given by

$$\begin{aligned}\varphi(d,\psi,k_z)\approx&\psi-d\omega_c/v_\zeta{}^0+2\sum_{n\geq 1}\left(\frac{v_\zeta{}^n}{nv_\zeta{}^0}\right)\sin\left(\frac{n\omega_c d}{2v_\zeta{}^0}\right)\\ &\times\cos\left(n\psi-\frac{n\omega_c d}{2v_\zeta{}^0}-\psi_\zeta{}^n\right).\end{aligned}\tag{13a}$$

This calculation assumed that the sum of the oscillatory terms is much smaller than the leading term ($\psi-\varphi\gg 2\pi$) and involved a single iteration of Eq. (6) using Eq. (11). Since we here neglect all discontinuities in φ, i.e., the places on a trajectory where $v_\zeta(\psi)=0$, we can average over all starting points (see discussion in Sec. VI) and keep only the nonoscillatory part of Eq. (13a).

Substituting Eqs. (11) and

$$\varphi(d,\psi,k_z)\approx\psi-d\omega_c/v_\zeta \tag{13b}$$

into Eq. (10), we find after much calculation

$$\sigma_{ij}=\sigma_{ij}{}^0+\Delta\sigma_{ij}, \tag{14}$$

[16] We should actually integrate over both ζ and ξ axes and divide by the sample area. Then we need to consider the effective area of electrons contributing to oscillatory conductivity and bulk conductivity. This is done in Sec. VI (see Fig. 1, bottom).

[17] I. M. Lifshitz, M. Ya, Azbel, and M. I. Kaganov, Zh. Eksperim. i Teor. Fiz. 31, 63 (1956) [English transl.: Soviet Phys.—JETP 4, 41 (1957); I. M. Lifshitz, and M. I. Kaganov, Usp. Fiz. Nauk 87, 389 (1965) [English transl.: Soviet Phys.—Usp. 8, 805 (1966)].

[18] H. Stolz, Phys. Status Solidi 3, 1153 (1963).

where the nonoscillatory part of the conductivity tensor is given by

$$\sigma_{ij}^{0}(\zeta)=\frac{4e^2}{h^2}\int_{v_\zeta^0>0} dk_z m^*\tau v_i^0 v_j^0\left[1-\frac{v_\zeta^0\tau}{d}(1-e^{-d_\zeta/v_\zeta^0\tau})\right]+\frac{8e^2}{h^2}\int_{v_\zeta^0>0} dk_z m^*\tau\sum_{n\geq 1}\left\{\left[1-\frac{v_\zeta^0\tau}{d_\zeta}\frac{1-(n\omega_c\tau)^2}{1+(n\omega_c\tau)^2}\right]\times\frac{\mathrm{Re}(v_i^{(-n)}v_j^{(n)})}{1+(n\omega_c\tau)^2}+\left[1-\frac{v_\zeta^0\tau}{d}\frac{2n\omega_c\tau}{1+(n\omega_c\tau)^2}\right]\frac{n\omega_c\tau\,\mathrm{Im}(v_i^{(-n)}v_j^{(n)})}{1+(n\omega_c\tau)^2}\right\}, \quad (15)$$

and the part of the conductivity tensor which oscillates with the magnetic field is given by

$$\Delta\sigma_{ij}(d_\zeta)=\frac{2e^2}{h^2 d}\int dk_z m^* v_\zeta^0\tau^2 e^{-d_\zeta/v_\zeta^0\tau}\times\sum_{n\geq 1}\frac{v_i^n v_j^n}{1+(n\omega_c\tau)^2}\cos[nd_\zeta\omega_c/v_\zeta^0+\varphi_{ij}^n]. \quad (16)$$

Notice that in Eqs. (12), (13), (15), (16), and following, the k_z dependence of the quantities is implicit. The phase shift occurring in Eq. (16) is given by

$$\varphi_{ij}^n=\arcsin\left[\frac{2n\omega_c}{1+(n\omega_c\tau)^2}\right|+\arcsin\left|\frac{\mathrm{Im}(v_i^{(-n)}v_j^{(n)})}{|v_i^{(-n)}||v_j^{(n)}|}\right]. \quad (17)$$

The second term in Eq. (17) represents the phase shift from the diagonal to the off-diagonal components of the oscillations in the conductivity tensor; it is $\frac{1}{2}\pi$ only if the angle $|\psi_i^n-\psi_j^n|=\frac{1}{2}\pi$ which happens when the orbit has reflection symmetry through a line. The magnetic-field-dependent phase shift [the first term in Eq. (17)] is negligible for large $\omega_c\tau$.

Now, in general, both v_ζ^0 and $m^*v_\zeta^0$ are functions of k_z. The most critical parameter is $m^*v_\zeta^0$ which appears as both argument and coefficient in the oscillatory terms. For closed orbits

$$m^*=\frac{\hbar^2}{2\pi}\left(\frac{\partial A}{\partial\epsilon}\right)_{k_z},\quad v_\zeta^0=\hbar^{-1}\cos\theta\left(\frac{\partial\epsilon}{\partial k_z}\right)_A, \quad (18)$$

where A is the area of the electron orbit in k space. In all the formulas except Eq. (18), m^* should be taken as the magnitude of the orbital mass [so that Eq. (4) gives $|m^*|$]. Therefore in the following equations the negative of the m^* defined in Eq. (18) should be used for holes [so, $-(\partial A/\partial k_z)_{\epsilon_F}$ of Eq. (20) and subsequent expressions should be replaced by $+(\partial A/\partial k_z)_{\epsilon_F}$ in the case of holes]. For open orbits the area is not a well-defined concept, and it can be shown that

$$(m^*v_\zeta^0)_{\mathrm{open}}=\cos\theta\,(m^*v_z^0)_{\mathrm{open}}+\sin\theta\,(\hbar K_y/2\pi), \quad (19)$$

where the second term in Eq. (19) only exists if the periodicity vector $\hbar\mathbf{K}$ for the open surface [we consider only "periodic open surfaces"[14,18] for which the periodic expansion of Eq. (11) and an effective mass like that of Eq. (4) are valid] in $\mathbf{k}$ space points along the y axis (the axis orthogonal to the plane determined by the z and ζ axes; see Fig. 1).

Limiting our discussion here to closed orbits, asymptotic considerations of the large parameter (we are considering large fields),

$$n\omega_c d/v_\zeta^0=\frac{neHd_\zeta}{cm^*v_\zeta^0}=-\frac{2\pi neHd_\zeta}{ch\cos\theta}\left(\frac{\partial A}{\partial k_z}\right)_{\epsilon_F}^{-1}=\frac{2\pi nH}{\Delta H}, \quad (20)$$

show that dominating contributions to the integral in Eq. (16) arise from (1) regions where $(\partial A/\partial k_z)_{\epsilon_F}$ is constant over a finite k_z range Δk_z; (2) stationary points k_z^* where $(\partial A/\partial k_z)_{\epsilon_F}$ is an extremum as a function of k_z; (3) limiting points or cutoff orbits where k_z is extreme (end of the k_z integration).

The first type of contribution (from k_z^0 to $k_z^0+\Delta k_z$) yields

$$\Delta\sigma_{ij}^{(1)}\approx 2\left(\frac{c}{\pi H}\right)^2\frac{h\Delta k_z}{d_\zeta\sec\theta}\left(\frac{-1}{2\pi}\frac{\partial A}{\partial k_z}\right)^3\sum_{n\geq 1}\left|\frac{1}{\Delta k_z}\times\int_{k_z^0}^{k_z^0+\Delta k_z} dk_z\exp[-d_\zeta\sec\theta/v_\zeta^0\tau]\frac{v_i^{(-n)}v_j^{(n)}}{(nv_z^0)^2}\right|\times\cos\left(\frac{2\pi nH}{\Delta H}+\theta_{ij}^n\right). \quad (21)$$

The phase shift in the cosine of Eq. (21) is given by

$$\sin\theta_{ij}^n=\left[\int_{k_z^0}^{k_z^0+\Delta k_z} dk_z\exp[-d_\zeta\sec\theta/v_z^0\tau]\times\frac{v_i^n v_j^n}{(nv_z^0)^2}\sin\varphi_{ij}^n\right]\times\left[\left|\int_{k_z^0}^{k_z^0} dk_z\exp[-d_\zeta\sec\theta/v_z^0\tau]\frac{v_i^{(-n)}v_j^{(n)}}{(nv_z^0)^2}\right|\right]^{-1}. \quad (22)$$

The second type [evaluated at k_z^* where $(\partial^2A/\partial k_z^2)_{\epsilon_F}$] yields[19]

$$\Delta\sigma_{ij}^{(2)}\approx\pi\left[e\left|\left(\frac{\partial^3A}{\partial k_z^3}\right)_{\epsilon_F}\right|(d_\zeta\sec\theta/\hbar)^3(\pi H/c)^5\right]^{-1/2}\times\left(\frac{-1}{2\pi}\left(\frac{\partial A}{\partial k_z}\right)_{\epsilon_F}\right)^4\exp[-(d_\zeta\sec\theta)/v_z^0\tau]\times\sum_{n\geq 1}\frac{v_i^n v_j^n}{n^{5/2}(v_z^0)^2}\cos\left(\frac{2\pi nH}{\Delta H}+\varphi_{ij}^n\mp\tfrac{1}{4}\pi\right), \quad (23)$$

[19] A. Erdelyi, *Asymptotic Expansions* (Dover Publications, Inc., New York, 1956).

where the $\mp\frac{1}{4}\pi$ phase shift corresponds to the "acceleration" $(\partial^3 A/\partial k_z^3)_{\epsilon_F}$ being negative or positive, respectively. Note that we are considering $v_z{}^0>0$, and since m^* is positive (negative), $-(\partial A/\partial k_z)_{\epsilon_F}$ is positive (negative) for electrons (holes) [see Eqs. (10) and (18)]. However, recall from the discussion after Eq. (18) that in all the formulas we must take m^* and $-(\partial A/\partial k_z)_{\epsilon_F}$ as positive for both electrons and holes [so that the above criterion applies to $-(\partial^3 A/\partial k_z^3)_{\epsilon_F}$ in the case of holes]. The $H^{-5/2}$ dependence of the amplitude in Eq. (23) agrees with Gurevich's calculation[7] but not that of Grenier *et al.*[8] who stated an $H^{-7/2}$ law. Note that this type of oscillation (occurring for non-ellipsoidal FS) is sinusoidal, contrary to the expectations of Gurevich.

The third type (from limiting point electrons where **v** is parallel to the k_z axis) yields

$$\Delta\sigma_{ij}{}^{(3a)}\approx 2e^2(\hbar/d_\zeta\sec\theta)^3\left(\frac{c}{eH}\right)^4 \times\left(\frac{-1}{2\pi}\left(\frac{\partial A}{\partial k_z}\right)_{\epsilon_F}\right)^7\left(\frac{\partial^2 A}{\partial k^2{}_z}\right)^{-2}\exp[-(d_\zeta\sec\theta)/v_z{}^0\tau] \times\sum_{n\geq 1}\frac{\partial/\partial k_z(v_i{}^n v_j{}^n)}{n^4(v_z{}^0)^2}\cos\left[\frac{2\pi nH}{\Delta H}+\varphi_{ij}{}^n\right]. \quad (24)$$

In this case (FS elliptic limiting point) one can show that $(1/2\pi(\partial A/\partial k_z)_{\epsilon_F})^{-2}$ is equal to the local Gaussian curvature.[7] These types of contributions are similar to the original predictions of Sondheimer for a spherical FS. Discontinuous or truncated FS will also contribute terms which take the form

$$\Delta\sigma_{ij}{}^{(3b)}\approx\frac{e^2}{\pi}(\hbar/d_\zeta\sec\theta)^2\left(\frac{c}{eH}\right)^3\left(\frac{-1}{2\pi}\left(\frac{\partial A}{\partial k_z}\right)_{\epsilon_F}\right)^5 \times\left(\frac{\partial^2 A}{\partial k_z{}^2}\right)_{\epsilon_F}^{-1}\exp[-(d_\zeta\sec\theta)/v_z{}^0\tau] \times\sum_{n\geq 1}\frac{v_i{}^n v_j{}^n}{n^3(v_z{}^0)^2}\sin\left[\frac{2\pi nH}{\Delta H}+\varphi_{ij}{}^n\right]. \quad (25)$$

Examination of the above expressions [Eqs. (22)–(25), successively] show that in each case the frequency of the conductivity oscillations depends on $[-(\partial A/\partial k_z)_{\epsilon_F}/d_\zeta\sec\theta]^{-1}$ while the amplitude depends in part on the quantity

$$\exp[-(d_\zeta\sec\theta)/v_z{}^0\tau]\left(\frac{e}{\pi v_z{}^0}\right)^2(\hbar/d_\zeta\sec\theta)^{S-1} \times(c/eH)^S\left[\frac{-1}{2\pi}\left(\frac{\partial A}{\partial k_z}\right)_{\epsilon_F}\right]^{2S-1}, \quad (26)$$

where S is the number 2, $2\frac{1}{2}$, 4, and 3, respectively. Then in addition the amplitude of the nth Fourier component depends on the product of n^{-S} with

$$2\Delta k_z|v_i{}^{(-n)}v_j{}^{(n)}|,\quad\left|\frac{1}{\pi}\left(\frac{\partial^3 A}{\partial k_z{}^3}\right)_{\epsilon_F}\right|^{-1/2}v_i{}^n v_j{}^n,$$

$$\left[\frac{1}{\pi}\left(\frac{\partial^2 A}{\partial k_z{}^2}\right)_{\epsilon_F}\right]^{-2}\frac{\partial}{\partial k_z}(v_i{}^n v_j{}^n),\quad 2\left[\frac{1}{\pi}\left(\frac{\partial^2 A}{\partial k_z{}^2}\right)_{\epsilon_F}\right]^{-1}v_i{}^n v_j{}^n, \quad (27)$$

for Eqs. (22)–(25), respectively.

Equation (26) indicates that in a large magnetic field the temperature affects the amplitude only through the exponential factor involving the mean free path, and that the highest frequencies produce the strongest signals for oscillations of a given type; also Eq. (27) shows that for complicated orbits the data will contain higher harmonics whose amplitude depends on the Fourier coefficients of the velocity [Eq. (12)] divided by the Sth power of the harmonic number, and that the "density of orbits" on the FS contributing to the signal is determined in part by the size of the band: Δk_z, $(\partial^3 A/\partial k_z{}^3)_{\epsilon_F}{}^{-1}$, or $(\partial^2 A/\partial k_z{}^2)_{\epsilon_F}{}^{-1}$. Furthermore, the derivation of Eqs. (21) and (22) indicate that a dominating contribution from a finite size orbit can change its character as a function of magnetic field strength. This will happen when there is not strict parabolicity (regions of constant $\partial A/\partial k_z$ imply the existence of a dispersion law like $A\sim k_\perp{}^2\sim k_z$) but $|\partial^3 A/\partial k_z{}^3|\ll 1$. Then the oscillations will change from type (1) to type (2) as H increases through the value satisfying

$$\left(\frac{2\pi nH}{\Delta H}\right)\left|\left(\frac{\partial^3 A/\partial k_z{}^3}{\partial A/\partial k_z}\right)_{\epsilon_F}\right|(\Delta k_z)^2\sim\tfrac{1}{2}\pi$$

for finite Δk_z. This behavior will cause the amplitude dependence on H to change smoothly from H^{-2} to $H^{-2.5}$. Far more interesting is the change of character from type (2) to type (1) as a function of magnetic-field orientation. Suppose a slight rotation of the H direction changes an orbit which is strongly of type (2) [then the extremum in $(\partial A/\partial k_z)_{\epsilon_F}$ is sharp so that $(\partial^3 A/\partial k_z{}^3)_{\epsilon_F}$ is large] to one of type (1) (introducing paraboloidal or hyperboloidal behavior). This will cause a very sharp rise in the amplitude, the relative increase being given by

$$(\Delta\sigma_{ij}{}^{(1)}/\Delta\sigma_{ij}{}^{(2)})\sim\frac{16\pi nH}{\Delta H}\frac{|\partial^3 A/\partial k_z{}^3|_{\epsilon_F}{}^{(2)}}{(\partial A/\partial k_z)_{\epsilon_F}} \times[(\Delta k_z)^{(1)}]^2\gg 1, \quad (28)$$

where we have assumed that the frequency $(\partial A/\partial k_z)_{\epsilon_F}$ has not changed significantly in magnitude under the small rotation. Furthermore, the phase of the oscillations will abruptly shift by $\frac{1}{4}\pi$.

To obtain the magnetoresistivity one must invert the conductivity tensor; this necessitates the evaluation of Eq. (15) at large fields. We find for the diagonal

components

$$\sigma_{ii}^0(d_\xi)\approx\frac{4e^2}{h^2}\int_{v_\xi^0>0}dk_z m^*\tau(v_i^0)^2\left[1-\frac{v_\xi^0\tau}{d_\xi}(1-e^{-d_\xi/v_\xi^0\tau})\right]+2\left(\frac{c}{hH}\right)^2\int_{v_\xi^0>0}dk_z\frac{(m^*)^3}{\tau}\left(1+\frac{v_\xi^0\tau}{d_\xi}\right)\sum_{n\geq 1}\left(\frac{v_i^n}{n}\right)^2, \quad (29)$$

while for the off-diagonal components

$$\sigma_{ij}^0(d_\xi)\approx\frac{4e^2}{h^2}\int_{v_\xi^0>0}dk_z\, m^*\tau v_i^0 v_j^0\left[1-\frac{v_\xi^0\tau}{d}(1-e^{-d_\xi/v_\xi^0\tau})\right]+\frac{8ec}{h^2H}\int dk_z(m^*)^2\sum_{n\geq 1}(1-(n\omega_c\tau)^{-2})^{n-1}\,\mathrm{Im}(v_i^{(-n)}v_j^{(n)})$$
$$+8\left(\frac{c}{hH}\right)^2\int_{v_\xi^0>0}dk_z\frac{(m^*)^3}{\tau}\sum_{n\geq 1}n^{-2}\left[\left(1+\frac{v_\xi^0\tau}{d_\xi}\right)\mathrm{Re}(v_i^{(-n)}v_j^{(n)})-2\frac{v_\xi^0\tau}{d_\xi}\,\mathrm{Im}(v_i^{(-n)}v_j^{(n)})\right]. \quad (30)$$

Notice that for long mean free path, $v_\xi^0\tau\gg d$, the above expressions for σ^0 become independent of τ. Since we are concerned with samples having more than one dimension less than the mean free path, we must modify these formula for comparison with experiment[16,20]; however, this will not affect the magnetic field dependence shown in Eqs. (29) and (30). Inverting Eq. (14) yields, for the oscillatory part when H is in the ab plane (drift velocities existing along x and z directions), in the magnetic field coordinates

$$\Delta\rho=\Delta(\sigma^{-1})=(\det\sigma^0)^{-1}\begin{bmatrix}\sigma_{zz}^0\Delta\sigma_{yy} & -\sigma_{zz}^0\Delta\sigma_{xy} & -\sigma_{xy}^0\Delta\sigma_{yy}\\ -\sigma_{zz}^0\Delta\sigma_{yx}+\sigma_{zx}^0\Delta\sigma_{yz} & \sigma_{zz}^0\Delta\sigma_{xx}+\sigma_{xx}^0\Delta\sigma_{zz}-\sigma_{zz}^0\Delta\sigma_{xz}-\sigma_{xz}^0\Delta\sigma_{zx} & \sigma_{xz}^0\Delta\sigma_{yx}-\sigma_{xx}^0\Delta\sigma_{yz}\\ -\sigma_{zx}^0\Delta\sigma_{yy} & \sigma_{zx}^0\Delta\sigma_{xy}-\sigma_{xx}^0\Delta\sigma_{zy} & \sigma_{xx}^0\Delta\sigma_{yy}\end{bmatrix}. \quad (31)$$

Transforming to the laboratory (crystal) coordinates we need the expression for two of the components to compare with our experiment (J along c or y axis),

$$(\Delta\rho)_{cc}=(\det\sigma^0)^{-1}(\sigma_{zz}^0\Delta\sigma_{xx}+\sigma_{xx}^0\Delta\sigma_{zz}-\sigma_{zx}^0\Delta\sigma_{xz}-\sigma_{xz}^0\Delta\sigma_{zx}),$$
$$(\Delta\rho)_{bc}=-(\det\sigma^0)^{-1}[(\sigma_{zz}^0\cos\theta-\sigma_{zx}^0\sin\theta)\Delta\sigma_{xy}+\sigma_{xx}^0\sin\theta\Delta\sigma_{zy}]. \quad (32)$$

Note that when H is in the ab plane (J along c axis), $\det\sigma^0$ involves all the elements of the conductivity tensor, and for large fields goes as H^{-2}.

When H is exactly along the a axis and J is along the b axis, open orbits still exist (producing drift motion along b as well as a) and we find from Eq. (31)

$$(\Delta\rho)_{bb}=(\det\sigma^0)^{-1}\sigma_{aa}^0\Delta\sigma_{cc},$$
$$(\Delta\rho)_{cb}=-(\det\sigma^0)^{-1}(\sigma_{aa}^0\Delta\sigma_{cb}-\sigma_{ab}^0\Delta\sigma_{ca}). \quad (33)$$

However, if θ is not zero, H rotated into the ac plane (J along b or y axis), there no longer are open orbits and in the magnetic field coordinates

$$\Delta\rho=-(\sigma_{xy}^0\sigma_{yx}^0)^{-1}\begin{bmatrix}\Delta\sigma_{yy} & -\Delta\sigma_{xy}\\ -\Delta\sigma_{yx} & \Delta\sigma_{xx}\end{bmatrix}, \quad (34)$$

all other components being smaller by a factor $(\omega_c\tau)^{-1}$ in large magnetic fields. Then in the laboratory system we find

$$(\Delta\rho)_{bb}=-(\sigma_{xy}^0\sigma_{yx}^0)^{-1}\Delta\sigma_{xx},$$
$$(\Delta\rho)_{cb}=(\sigma_{xy}^0\sigma_{yx}^0)^{-1}\Delta\sigma_{xy}\cos\theta. \quad (35)$$

In this case of only closed orbits the $\det\sigma^0$, $-\sigma_{xy}^0\sigma_{yx}^0\sigma_{zz}^0$, also goes as H^{-2}.

When there is exact compensation between electrons and holes, a different result is obtained.[17] From Eq. (4) we have

$$\hbar\hat{z}\times d\mathbf{k}=-m^*\mathbf{v}_\perp d\psi.$$

Using Eq. (11) we can integrate the Lorentz equation,

$$\hbar(d\mathbf{k}/d\psi)=m^*\hat{z}\times\mathbf{v},$$

and obtain

$$\hbar\mathbf{k}_\perp=m^*z\times\sum_{n\geq 1}\frac{e^{in\psi}}{in}\mathbf{v}^{(n)}.$$

Then using Eq. (11) once again we find that the area of the orbit in k space can be expressed as

$$A(k_z)=\pm\tfrac{1}{2}\hat{z}\cdot\oint\mathbf{k}_\perp\times d\mathbf{k}$$
$$=\pm 4\pi(m^*/\hbar)^2\sum_{n\geq 1}n^{-1}\,\mathrm{Im}(v_x^{(-n)}v_y^{(n)}), \quad (36)$$

where $\pm$ means electrons/holes.

Thus, from Eq. (30) when only closed orbits exist,

$$\sigma_{xy}^0=\frac{2ec}{(2\pi)^3H}\left[\int_{\text{els}}dk_z A(k_z)-\int_{\text{holes}}dk_z A(k_z)\right]+\frac{1}{H^2}C_{xy}^{(2)}+\frac{1}{H^3}C_{xy}^{(3)}$$
$$=\frac{ce}{H}(n_1-n_2)+\frac{1}{H^2}C_{xy}^{(2)}+\frac{1}{H^3}C_{xy}^{(3)}, \quad (37)$$

[20] The oscillatory part $\Delta\sigma$ needs to be modified only by an angular-dependent factor which shows that the amplitude vanishes when H is along the sample diagonal. Neighboring trajectories connecting adjacent sample faces have different frequencies incoherent in phase and so do not contribute to $\Delta\sigma$. In Sec. VI we also consider the open orbits which can connect the opposite faces whose normal parallels the ξ axis.

where n_1 is the number of states occupied by electrons with positive effective mass, and n_2 the number of unoccupied states with negative effective mass.[17] According to Reed and Marcus, gallium is *almost* exactly compensated.[21] Therefore, we need an expression for the determinant of σ^0 for a *partially compensated* metal [from Eqs. (29), (30), and (37)]:

$$\det\sigma^0 \approx \tfrac{1}{4}C_{zz}^{(0)}H^{-4}\{(2(n_1-n_2)ecH+C_{xy}^{(2)}-C_{yx}^{(2)})^2-(C_{xy}^{(2)}+C_{yx}^{(2)})(C_{xy}^{(2)}+C_{yx}^{(2)}-4C_{xz}^{(1)}C_{zy}^{(1)}/C_{zz}^{(0)}) +4(C_{xx}^{(2)}C_{yy}^{(2)}-C_{xz}^{(1)}C_{zx}^{(1)}C_{yy}^{(2)}/C_{zz}^{(0)}-C_{xx}^{(2)}C_{yz}^{(1)}C_{zy}^{(1)}/C_{zz}^{(0)})\}^{-1}\equiv\tfrac{1}{4}C_{zz}^{(0)}H^{-4}D^{-1}. \quad (38)$$

Here the parenthesized superscript (n) indicates the coefficient of the $1/H^n$ term of the conductivity tensor. Equation (34) is replaced then by

$$\rho=4H^2D\begin{bmatrix} C_{yy}^{(2)}-C_{yz}^{(1)}C_{zy}^{(1)}/C_{zz}^{(0)}+H^2\Delta\sigma_{yy} & -C_{xy}^{(2)}+C_{xz}^{(1)}C_{zy}^{(1)}/C_{zz}^{(0)}-(n_1-n_2)ecH \\ & -H^{-1}C_{xy}^{(3)}-H^2\Delta\sigma_{xy} \\ -C_{yx}^{(2)}+C_{zx}^{(1)}C_{yz}^{(1)}/C_{zz}^{(0)}+(n_1-n_2)ecH & C_{xx}^{(2)}-C_{xz}^{(1)}C_{zx}^{(1)}/C_{zz}^{(0)}+H^2\Delta\sigma_{xx} \\ -H^{-1}C_{yx}^{(3)}-H^2\Delta\sigma_{yx} & \end{bmatrix}. \quad (39)$$

For the case of the *compensated* metal, then, the growth of the magnetoresistance is quadratic in H whether or not the open orbits have been excited. However, the leading term for open orbit off-diagonal resistivity goes as H (Hall voltage) while if no open orbits have been excited, the off-diagonal resistivity depends quadratically on H (transverse-even voltage[21]) and the Hall voltage has a linear-plus-weak (because $n_1-n_2\approx 0$) cubic dependence on H.[22]

For strong magnetic fields [but no so large that the H-dependent term in D of Eq. (38) grows larger than the constant ones] a profound change in the amplitude of $\Delta\rho$ will be observable as the magnetic field is rotated in and out of the ab plane. This is evident upon comparing Eq. (32), $\Delta\rho\sim H^2\Delta\sigma$ with Eq. (39) $\Delta\rho\sim H^4\Delta\sigma$. The open orbits in gallium exist only over a thin band in k space[21] (see discussion in Sec. VI). Therefore, a slight misorientation of H will transform the metal from the normal behavior [open orbit or uncompensated metal, Eqs. (31) and (34)] to the "abnormal" behavior of a compensated metal: Eq. (39) indicates growth to saturation for Sondheimer orbits, case (3a), and quadratic growth for paraboloidal orbits, case (1). Since we are dealing with very pure samples wherein the sample dimensions are smaller than the mean free path, the question of the interaction of *almost* open trajectories (extended orbits) with the boundaries becomes important. This will be discussed in Sec. VI.

Recall again that we have neglected the effects of any oscillations along ζ which alter the time of transit in the sample. Oscillations in the resistivity can result from oscillations in the time of flight between the parallel faces as well as the spatial oscillations of the electron during that time. An investigation showed that they alter the line shape slightly (no longer purely sinusoidal) but do not alter the amplitude dependence on H significantly. In fact, when $|v_\zeta^{\rm osc}/v_\zeta^0|\gtrsim 1$, some extra oscillation with possible sharp discontinuities in slope will occur. These are due to fitting into the metal chains of oscillating electrons having $v_\zeta=0$ at the beginning and end of their trajectories. This spatial resonance (rather than the temporal one discussed here) becomes the dominant feature in the Gantmaker effect.[23] There the current concentrated in the rf skin depth (an order of magnitude smaller than the sample thickness) is carried across the metal by the electrons.

III. EXPERIMENTAL DETAILS

Single-crystal specimens were grown in carefully machined Plexiglas Schubinkov molds from 99.9999% purity gallium supplied by the Aluminum Company of America (ALCOA). Internal surfaces were wiped successively with acetone, and alcohol, and given a light coating of Dow Corning DC200 silicone oil before assembly to facilitate removal of the crystal. The mold was loosely stoppered at one end and injected with gallium, heated to about 80°C in dilute HCl. A small seed crystal of the required orientation was placed in contact with the liquid column, and a temperature gradient established across the mold. The growth of the 15-cm-long crystal required approximately 1 h; then the mold was disassembled and the sample carefully removed.

The location of the crystallographic axes with respect to the faces of the samples was checked by x-ray diffraction, and misalignment held to less than 1° in all cases. Current connections were made with $\frac{1}{8}$-in. copper ribbon tinned with gallium, and pairs of No. 38 potential leads spot welded to each face as described by Yahia.[24]

Figure 2 is a block diagram of the electrical circuitry, used to record both the magnetoresistive potentials and

[21] W. A. Reed and J. A. Marcus, Phys. Rev. **126**, 1298 (1962).

[22] The observations for a particular orientation of cadmium of the oscillatory conductivity by Grenier *et al.* (Ref. 8). [$H^4\Delta\sigma$ having constant amplitude at large fields; see our Eq. (24)] and the oscillations in the off-diagonal resistivity ρ_{xy} seen by H. J. Mackey, J. R. Sybert, and J. T. Fielder, Phys. Rev. **157**, 578 (1967) [$\Delta\rho_{xy}$ having constant amplitude at large fields; see our Eqs. (24) and (39)] are to be explained as Sondheimer oscillations (limiting-point electrons) in a compensated metal. The fact that Mackey *et al.* observe both ρ_{xx} and ρ_{xy} going as H^2 in high fields also shows they are dealing with a compensated metal.

[23] V. F. Gantmakher, Zh. Eksperim. i Teor. Fiz. **42**, 1416 (1962) [English transl.: Soviet Phys.—JETP **15**, 982 (1962)].

[24] J. Yahia, Ph.D. thesis, Northwestern University, Evanston, Ill., 1958 (unpublished).

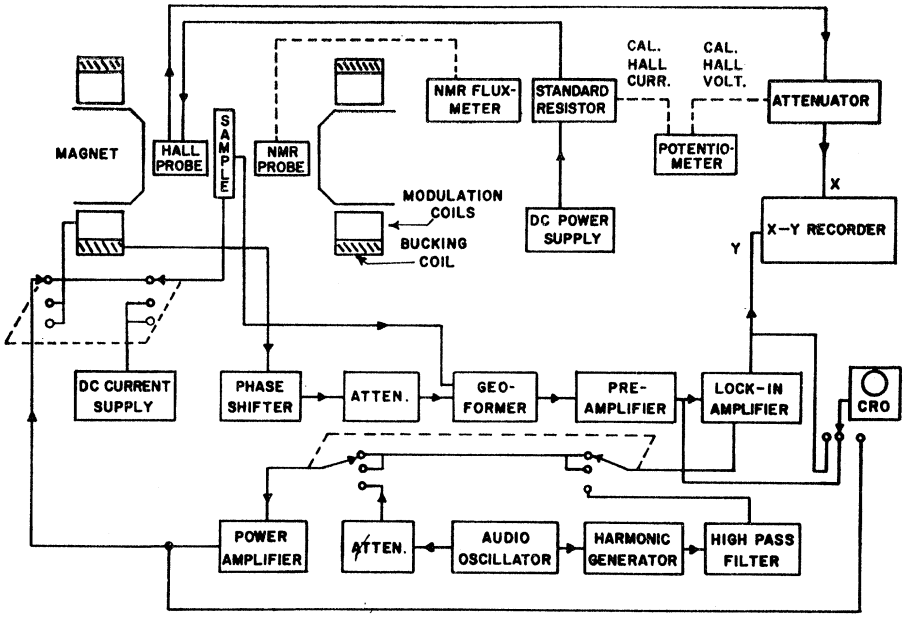

FIG. 2. Block diagram of the experiment.

their first and second derivatives with respect to magnetic field. The dc magnetic field was modulated by a small, parallel, audio-frequency component $H_1 \cos 2\pi ft$, of 10 to 100 Oe at 36 Hz. It can be shown[25] that for small modulation, $H_1 \ll \Delta H$, where ΔH is the period of the data, the signal appearing at the nth harmonic of the driving frequency is directly proportional to the nth derivative of the resistance with respect to the magnetic field $(\partial^n R_{ij}/\partial H^n)$.

A 4-in. Weiss-type electromagnet, fitted with 500 turn-modulation coils provided a maximum static field of 16 kOe. Most of the measurements were made between 1.5 and 11.0 kOe to minimize mixing with de Haas–Schubnikov signals which are comparable in amplitude to the size effect in the higher field range.

Sample potentials were selected by an eight-position rotary switch and mixed with a bucking signal of appropriate phase and amplitude to cancel the residual pickup in the lead pairs. Coupling to the preamplifier, by means of a low-level impedance-matching transformer, provided electrical isolation of the sample and suppression of the dc signal component. The signal was further amplified, synchronously detected, filtered, and recorded on an X-Y plotter as a function of the magnetic field. The data were simultaneously recorded in digital form at 1000 points with a Datex processor.

The magnetic field readout was provided by a high-linearity Hall probe, which, suitably loaded, was accurate to within $\frac{1}{4}\%$ in the specified range. The correct termination resistor was chosen by comparing the Hall output with a Rawson rotating-coil gaussmeter, and the final calibration obtained by locating several field points with NMR. Precision of the frequency determination was limited to about 1%, primarily by drift in the control current of the Hall sensor.

IV. EXPERIMENTAL RESULTS

The oscillatory effects described here were first found during a series of exploratory measurements on samples previously used for a detailed investigation of the monotonic magnetoresistance by Reed and Marcus.[21] These specimens were square rods with 1-mm^2 cross section, and had residual resistance ratios of about 20 000 between room temperature and 4.2°K. At the time of the present experiments, however, higher purity material was available from ALCOA, and a new set of crystals was prepared which resulted in significantly improved residual resistance ratios[26] (see Table I). Frequency measurements described in this section were made on the latter at 1.2°K. Sample $C1$ corresponds roughly in size and shape to the specimens used by Reed and Marcus but has a ratio measured at 4.2°K of nearly 40 000, and more than 60 000 at 1.2°K, indicating that the resistivity has not saturated at 4.2°K. Samples $CA1$ and $CB1$, approximately half as thick, have a smaller ratio at 4.2°K of only 30 000 because of enhanced boundary scattering. In Sec. II we mentioned that when the mean free path l is comparable or longer than the sample dimensions, the conductivity becomes weakly dependent on l and more strongly dependent on the sample size. In the last paragraph in this section we show that a smaller sample is expected to have a higher resistivity.

The nature of the variation of the transverse magnetoresistance with magnetic field is illustrated in Fig. 3

[25] J. A. Munarin, Ph.D. thesis, Northwestern University, Evanston, Ill., 1966 (unpublished).

[26] C. S. Barrett, *Advances in X-Ray Analysis* (Plenum Press, Inc., New York, 1962), Vol. 5.

TABLE I. Sample dimensions and residual resistivity data.

Sample	d_a(mm) 293°K	d_a(mm) 2.35°K [a]	d_b(mm) 293°K	d_b(mm) 2.35°K	d_c(mm) 293°K	d_c(mm) 2.35°K	$\rho_{293°K}$ (10^{-6} Ω cm)	$\rho_{4.2°K}$ (10^{-10} Ω cm)	$\rho_{293°K}/\rho_{4.2°K}$	$\rho_{1.2°K}$ (10^{-10} Ω cm)	$\rho_{293°K}/\rho_{1.2°K}$
$C1$	0.981	0.980	0.998	0.990	20	···	48.8	12.30	39 700	8.08	60 500
$CB1$	0.894	0.893	0.544	0.539	20	···	48.2	16.05	30 000	10.42	46 200
$CA1$	0.532	0.531	0.899	0.891	20	···	···[b]	···	···	···	···
$B1$	0.935	0.934	20	···	0.930	0.926	6.63	1.73	38 400	···	···
$CR1$	$\bar{d}_{293°K}=1.47$		$\bar{d}_{2.35°K}=1.46$		20	···	44.8	10.90	41 100	···	···

[a] The sample dimensions at 2.35°K were computed using Barrett's x-ray diffraction values of the lattice parameters at room temperature and at 2.35°K (Ref. 26). The differential contraction in length $\Delta L/L$ between the two temperatures is -1.02×10^{-3}, -8.37×10^{-3}, and -4.12×10^{-3}, for the a, b, and c axes, respectively.

[b] Sample $CA1$ was accidently destroyed before accurate resistivity measurements were made, but the ratio $\rho_{293°K}/\rho_{4.2°K}$ was approximately 30 000.

for sample $C1$. Here the current runs parallel to the c axis, and the magnetic field is perpendicular to the a-axis face of the crystal, corresponding to the Sondheimer geometry. Plots (a), (b), and (c) represent the direct magnetoresistance, the first, and the second derivatives, respectively. Note that the oscillations in (b) and (c) are not discernible in the direct measurement (a). Representing the resistaace as the sum of the monotonic component $R_{ij}(H)$ quadratic in the field H and an oscillating part $\Delta R_{ij}(H)$, the ratio $\Delta R_{ij}(H)/R_{ij}(H)$ goes as H^{-2}, and from Fig. 3[plot (b)], is about 1 part in 5000 at 5 kOe.

The complexity of the oscillations, evident in Fig. 3(c), severely restricted the use of visual reduction methods. Even when coupled with electronic filtering techniques which have recently been described,[27,28] it is difficult to discriminate several periodic components differing by only a few percent because the filter pass band cannot be narrowed sufficiently. Therefore, the data were recorded directly in digital form and numerically integrated to yield the Fourier transform[29] for a preselected range of frequencies covering 1 to 15 $(\text{kOe})^{-1}$. According to Rayleigh's criterion,[30] two neighboring frequencies are just resolved when $(\Delta F/F)$ is equal to $1/n$, where n is the number of periods included in the integration interval. Separation of two branches of equal amplitude differing only by 1% in frequency therefore requires 100 or more cycles of data, which was usually the case for the primary data.

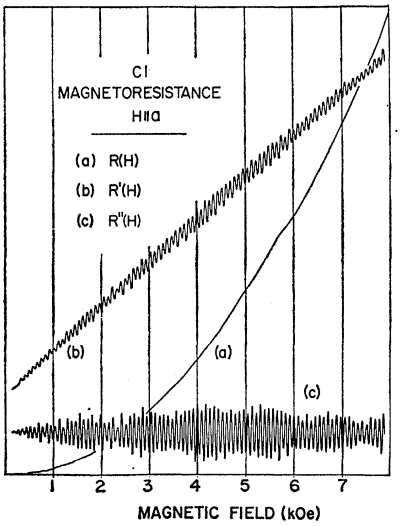

FIG. 3. Transverse magnetoresistance, sample $C1$. Curve (a) is a direct plot of $R(H)$. Curves (b) and (c) are first and second derivatives with respect to the magnetic field obtained by field modulation.

ab Plane

With the current J parallel to the c axis (c type), the transverse magnetoresistance oscillated with H for virtually any orientation of the magnetic field within the (transverse) ab plane, although the effects were strongest within 15° of the a axis. The specimens were, in all cases, oriented with the crystallographic axes perpendicular to the lateral faces, so that H parallel to either a or b for the c-type specimens corresponds to the Sondheimer geometry.

Typical field-sweep data for sample $C1$ are shown in Fig. 4 for tilt angles of 0°, 15°, 35°, 63°, and 72° measured from the a axis. The second harmonic is recorded in each case, and the accompanying plots give the Fourier spectrum.

For $\theta=0°$, five frequency terms are present within the range 10.0 to 14.0 kOe^{-1}, labeled $F1$ through $F5$ for reference, in order of increasing frequency.

At 15° the oscillation amplitude reaches an absolute maximum, and $F2$ strongly beats with an additional term $F6$. Here the sensitivity of the vertical scale in the data plot is reduced $2\frac{1}{2}$ times.

Periods $F2$, $F3$, and $F6$ are all comparable in size (13.3, 13.7, and 14.1 kOe^{-1}) and amplitude at 35° creating a complicated three-way beat pattern. Beyond this angle, the signal amplitude falls off rapidly, approaching a minimum at about 45°, near the diagonal of the sample (see Sec. VI).[20]

Period $F6$ is still observed at 63° but new periods of 4.2, 6.0, and 6.4 kOe^{-1} appear. Slow fluctuations in the

[27] A. Goldstein, S. J. Williamson, and S. Foner, Rev. Sci. Instr. **36**, 1356 (1965).

[28] J. B. Ketterson and Y. Eckstein, Rev. Sci. Instr. **37**, 44 (1966).

[29] The computer program was adapted from a de Haas–van Alphen reduction scheme due to J. Graebner [see J. Graebner, Ph.D. thesis, Northwestern University, 1967 (unpublished)].

[30] F. A. Jenkins and H. E. White, *Fundamentals of Optics* (McGraw-Hill Book Co., New York, 1957), p. 300.

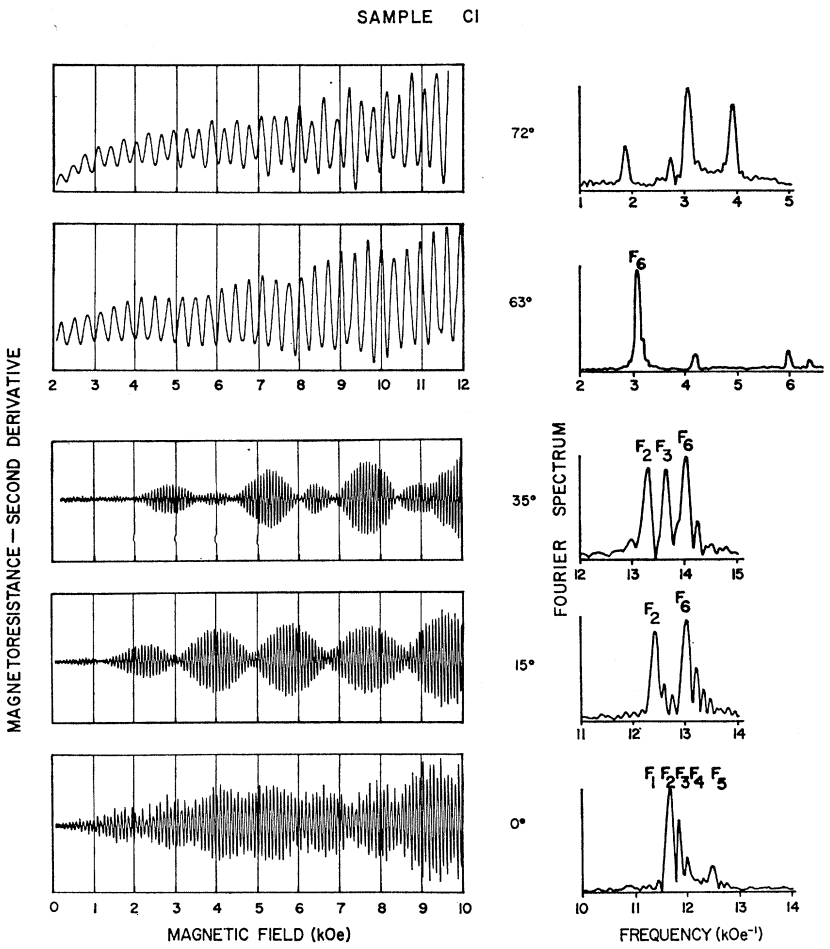

FIG. 4. Field-sweep data for sample *C*1 with H in the ab plane for $\theta_a = 0°$ (relative amplitude 1), 15° (relative amplitude was $2\frac{1}{2}$ times larger), 35° (relative amplitude 1), 63° (relative amplitude was 36 times smaller), and 72° (relative amplitude was 36 times smaller). The frequency spectrum obtained for each curve is shown to the right. Note the change of horizontal scale at the two largest angles.

baseline, about 2.5-kOe long are attributed to the difference frequency 0.4 kOe^{-1} between the two higher spectral terms. Here the amplitude of the oscillations is considerably smaller than for 0°, and the vertical sensitivity is increased by a factor of 36.

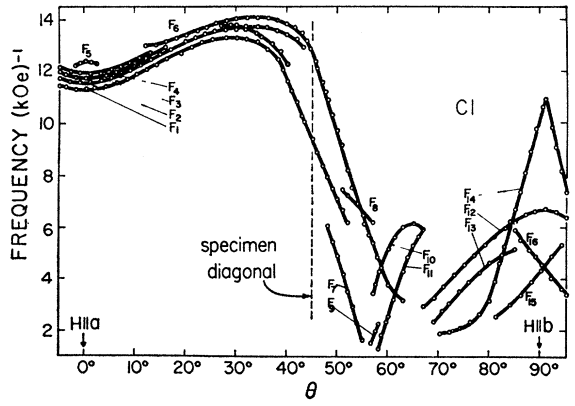

FIG. 5. Frequency spectrum for sample *C*1 with H in the ab plane. At 44.7° the magnetic field is parallel to the diagonal of the sample.

At 72°, another set of oscillations are present with frequencies 1.9, 3.0, and 3.9 kOe^{-1}. The oscillations become considerably weaker as the magnetic field is tipped toward the b axis (90°), although a number of distinct periods are still resolvable.

The complete frequency spectrum determined by Fourier analysis for this sample is presented in Fig. 5. The group of primary periods $F1$ through $F4$ have a relative minimum at 0°, rising through an absolute maximum at about 25°. $F6$ appears abruptly at 12°, and follows the first set very closely for $\theta > 20°$. Measurements in the neighborhood of 45° (near the diagonal) are difficult because of the low signal level, and only $F1$ and $F6$ can be resolved. For greater values of θ, other low-amplitude branches are observed within rather limited angular ranges and are designated $F7$ through $F16$.

The relative magnitude of each of the primary terms can be estimated from Fig. 6. This plot was made by computing the average value of the Fourier transform in the interval 1.5 to 11.0 kOe; assuming the amplitude growth is linear over this interval (see Fig. 7), it represents the relative sizes of the branches approximately

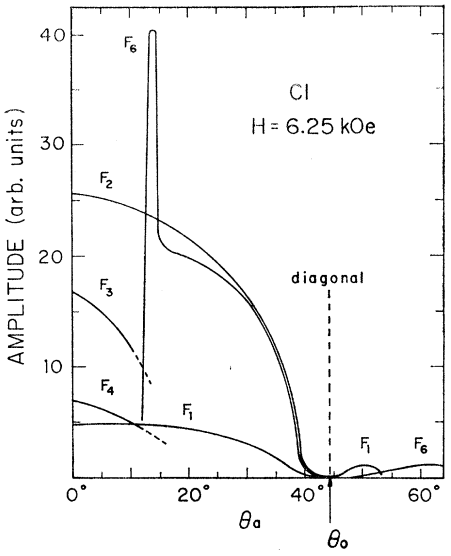

FIG. 6. Second derivative amplitude, sample *C*1. Note the vanishing amplitude for all frequency branches at the diagonal.

at the midpoint, i.e., 6.25 kOe. The set *F*1, *F*2, *F*3, and *F*4 have an amplitude maximum at 0° and fall off towards zero at the diagonal of the sample.[20] *F*6, however, has a sharp maximum at 15°, possibly related to an increase in the number of extremal orbits on the Fermi surface. Beyond θ_0, *F*1 and *F*6 appear, but with greatly reduced amplitude.

Oscillations in the Hall voltage were found only within a narrow range of $\pm 2°$ about the axis in this specimen. A phase shift of $\frac{1}{2}\pi$ between the magneto-

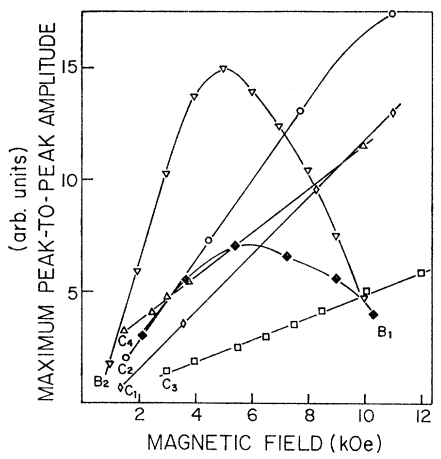

FIG. 7. The maximum peak-to-peak amplitude of magnetoresistance second derivative versus magnetic field strength. Curves *B*1 and *B*2 were measured from data taken with crystals which were sandblasted so as to produce surface irregularities of the size of the sand particles (23 μ). Curve *B*1 is from Fig. 1 of Ref. 10; curve *B*2 is from Fig. 20 of this paper. In both cases *H* is 7° from the *a* axis in the *ac* plane. Curve *C*1 is from unpublished data on sample *C*1 with *H* 15° from *a* axis in *ab* plane; curve *C*2 is from Fig. 1 of Ref. 10 for *H* 20° from *a* axis in *ab* plane; curves *C*3 and *C*4 are from Fig. 4 of this paper, *H* being 63° and 0° from *a* axis, respectively.

resistive and Hall potentials is expected on theoretical grounds (see Sec. II), but it is difficult to measure experimentally because of the complex beat structure (see Fig. 8). There is indication that this condition is fulfilled at least for the dominant term from both visual inspection of data such as in Fig. 8 and the fact that the off-diagonal oscillatory resistivity was found to be odd in current and magnetic field [see Eqs. (21) and (22)].

Shape and Size Dependence of Periods

Theoretical investigation of oscillatory size effects has heretofore been limited to the thin-film geometry in which the transverse dimensions in the plane of the film are assumed to be infinitely large. The observations of size effects for arbitrary orientation of the magnetic field in the present experiment, however, permit the relationship between the periodicity and sample geometry to be studied in detail. For this purpose *c*-type samples (current parallel to *c*) *CA*1 and *CB*1 with *rectangular* cross section were prepared (see Table I). The crystallographic *a* and *b* directions were aligned perpendicular to the lateral faces and the samples made identical in every respect except for the interchange of the two axes. The frequency spectra for these two specimens are plotted in Fig. 9. The plots are qualitatively similar to Fig. 5, except for some missing detail probably due to difficulties in sample preparation, since size effects depend very critically upon surface conditions as well as impurities and strain imperfections.

From Eq. (2) the frequency of the oscillations $F=1/H$, depends upon sample geometry through the factor $d\sec\theta$, where d is the thickness and θ is the angle between the magnetic-field direction and the perpendicular to the surface.

In the present case where both transverse sample dimensions are small compared to the mean free path, we must be careful to discern which pair of crystal faces are involved. For closed orbits this is determined by the angle between the sample diagonal and magnetic field, i.e., carrier drift, direction. Therefore, to make a direct comparison of the rectangular specimens, we

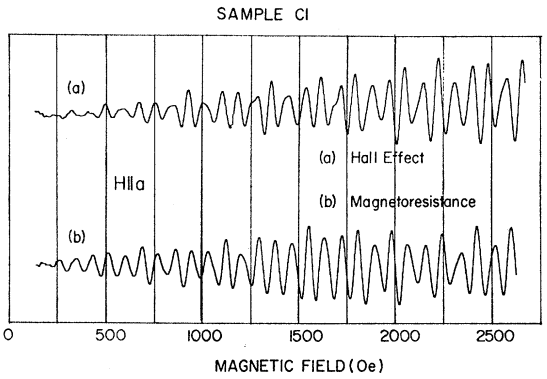

FIG. 8. Second derivative of Hall voltage curve (a) and resistivity curve (b), for sample *C*1.

TABLE II. Frequency data for sample $C1$ at the principal symmetry directions.

	$\mathbf{H}\|a(\theta_a=0°)$			$\mathbf{H}\|b(\theta_a=90°)$	
	F' (kOe mm)$^{-1}$	ΔH (Oe mm)		F' (kOe mm)$^{-1}$	ΔH (Oe mm)
F_1	11.6	86.2	F_{12}	6.7	149.0
F_2	11.8	84.8	F_{14}	10.6	94.4
F_3	12.0	83.4	F_{15}	4.3	233.0
F_4	12.1	82.7	F_{16}	4.6	217.0
F_5	12.6	79.4			

must plot the "reduced" frequency

$$F'=F/(d_a \sec\theta_a), \quad \theta_a<\theta_0$$
$$F'=F/(d_b \sec\theta_b), \quad \theta_a>\theta_0 \tag{40}$$

which should be independent of the size and shape of the cross section and depend only upon the Fermi-surface parameter $(\partial A/\partial k_z)_{eF}$. Here, θ_0 refers to the position of the diagonal relative to the indicated axis. The spectral data for the three samples $C1$, $CA1$, and $CB1$, plotted according to this scheme are given in Fig. 10. At the diagonal of either rectangular sample, the frequencies have a cusp and are approximately 15% too low. The lateral edges for these specimens, however, are not sharp but are rather rounded which means the quantity $d\sec\theta$ is smaller than the ideal value, invalidating the comparison in this region. Nonetheless, excluding the points near the respective corners of either sample, the results are consistent with Eq. (40) to

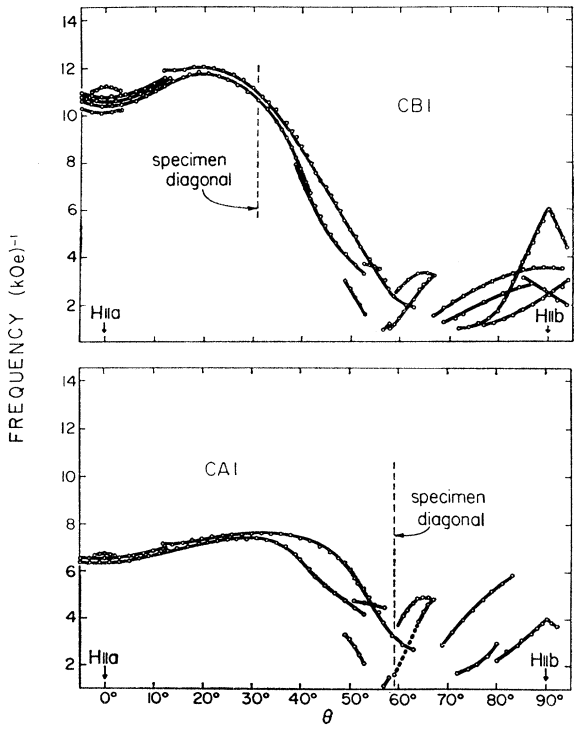

FIG. 9. Frequency spectra for samples $CA1$ (lower) and $CB1$ (upper). The diagonal θ_0 is located at 59.2° and 31.1, respectively.

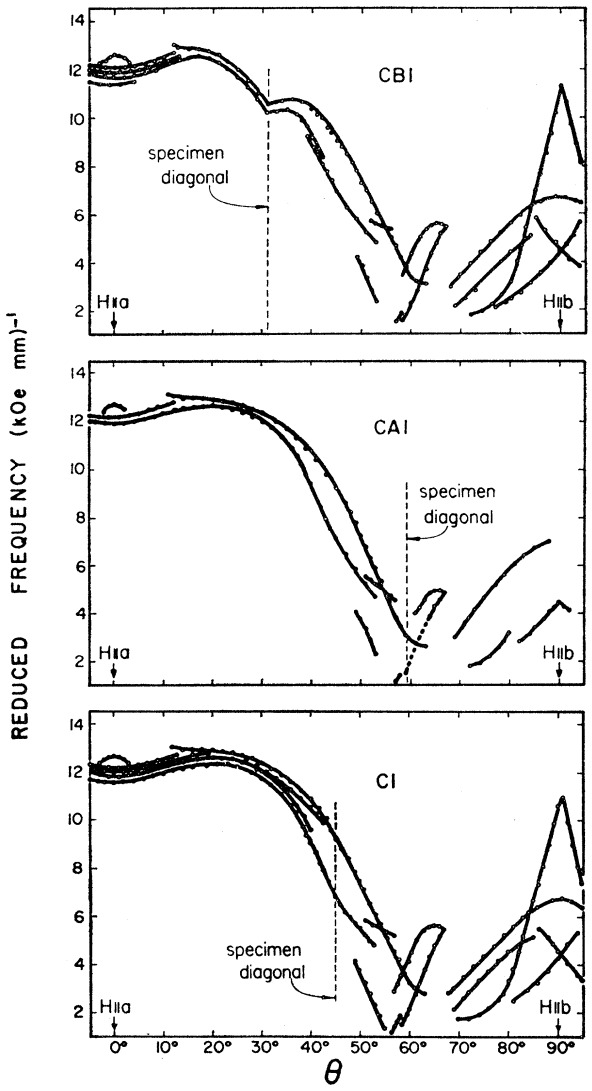

FIG. 10. Reduced frequency, samples $C1$, $CA1$, and $CB1$. Note the close correspondence except in the region of the diagonal for $CA1$ and $CB1$.

within experimental error (see Table II), and seem to establish that these effects are associated with closed trajectories on the Fermi surface.

Near the a axis, in sample $CB1$, an additional period, shown in Fig. 11, was observed which appears to be nearly a second subharmonic of the dominant oscillations. This frequency $F'=6.0$ (kOe mm)$^{-1}$ was of low amplitude and was not found in the other specimens, perhaps because of misalignment.

Additional measurements were made on a cylindrical sample $CR1$ with a diameter of 1.46 mm, and are shown in Fig. 12. Here the reduced frequency F' is given simply by F/d, where d is the diameter of the rod and the results are in agreement with the prior measurements. The amplitude of the oscillations, as expected, is very small, due to the large diameter and cylindrical

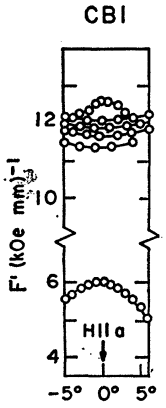

FIG. 11. Low-amplitude subharmonic period observed in sample *CB*1 with H in the *ab* plane.

geometry, but are easily discernible below 6 kOe. At higher fields, de Haas–Schubnikov oscillations growing exponentially in H, mask the size effect, since the latter is of relatively low amplitude. The reduced frequency is plotted in Fig. 13.

ac Plane

Measurements were made of the magnetoresistance and Hall-effect oscillations in *b*-type samples in the range $\theta_a \pm 38°$, where θ_a refers the angle between the magnetic field and the *a* axis measured in the plane perpendicular to the current (*ac*). We wish to point out that for these crystals the Hall oscillations were observed in a wide region of the *ac* plane (in contrast to the *c*-type samples) and were comparable in magnitude to the resistance oscillations at corresponding angles. The frequencies were identical for the two measurements, in some cases the data being clearer for the Hall oscillations. The spectrum of reduced frequencies for sample *B*1 is presented in Fig. 14. For $H \| a$, four periods have been identified: 11.2, 11.4, 11.5, and 18.1 kOe^{-1} (see Table III). The three lowest terms correspond to the group *F*1 through *F*4, but the additional high-frequency term 18.1 kOe^{-1} has not been found in the *c*-type samples. The connectivity of the various branches at 22° is ambiguous because of the large number of periods clustered together within a small range of frequency. The oscillations vanish beyond 38° and are not observed in the vicinity of the *c* axis.

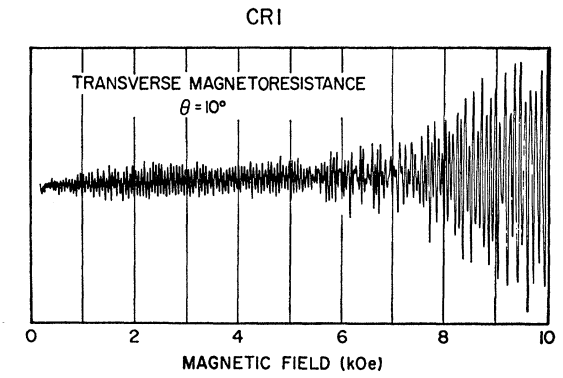

FIG. 12. Transverse magnetoresistance in the cylindrical sample *CR*1. The rapidly growing oscillations above 5 kOe are due to the de Haas–Schubnikov effect.

Temperature Dependence—Mean Free Path

For large magnetic fields according to the theory developed in Sec. II, the frequency of the oscillations should be independent of temperature, while the amplitude depends most strongly upon T through the factor $\exp[-(d \sec\theta)/l(T)]$, where $l(T)$ is the bulk mean free path of the conduction electrons. Thus, the logarithm of the amplitude of the oscillations is expected to follow the temperature behavior of the bulk resistivity which is inversely proportional to l. At low temperatures, the temperature dependent part of the resistivity due to normal electron-phonon interactions is proportional to T^5, and is ultimately dominated as $T \to 0$ by the electron-electron collisions which contribute a term proportional to T^2. Cochran and Yaqub[31] have found an empirical temperature dependence of $T^{2.4}$ for the ideal resistivity of gallium in the range 2.26 to 4.2°K, which presumably represents the combined effect of these two mechanisms. Plotting the amplitude versus $T^{2.4}$ in Fig. 15 gives good agreement with Cochran and Yaqub's results.

For zero magnetic field we find from Sec. II that when l is greater than or equal to the sample thickness, the conductivity

$$\sigma_i \sim \frac{2e^2}{h^2} \int dk_z \oint d\psi \frac{m^* d}{v_z(k_z,\psi)} v_i^2(k_z,\psi) \times \left[1 - \frac{1}{3}\frac{d}{\tau v_z(k_z,\psi)} + \frac{1}{12}\left(\frac{d}{\tau v_z(k_z,\psi)}\right)^2 - \cdots\right]. \quad (41)$$

This formula neglects scattering off the side walls of the sample since it was calculated for only one relevant

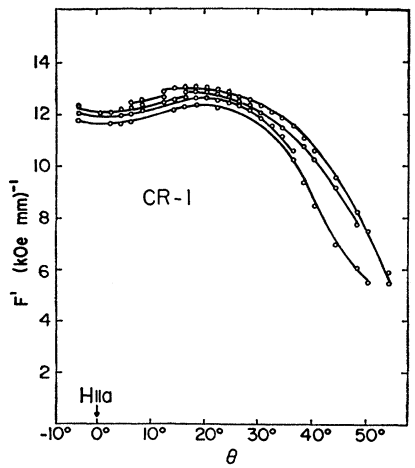

FIG. 13. Reduced frequency plot for cylindrical sample *CR*1.

[31] M. Yaqub and J. F. Cochran, Phys. Rev. **137**, A1182 (1965); **140**, A2174 (1965).

sample dimension. In the absence of a magnetic field both transverse directions are relevant and we can average two expressions like Eq. (41). Replacing τv_z by an effective mean free path l, we write

$$2l\sigma/\sigma_0 \sim d_1[1-\tfrac{1}{3}d_1/l+\tfrac{1}{12}(d_1/l)^2] + d_2[1-\tfrac{1}{3}d_2/l+\tfrac{1}{12}(d_2/l)^2], \quad (42)$$

where σ_0 is the bulk conductivity which is proportional to l. Substituting from Table I into this formula with $(4.2/1.2)^{2.4}$ equal to 20.2 and $l(1.2)/l(4.2)$, we find from the ratio of the resistivities ($\sim$1.5) that for sample $CB1$, $l(1.2)$ is 14 mm, while for sample $C1$, $l(1.2)$ is 18 mm. If one accepts these estimates, we find upon substituting back into Eq. (42) that a resistivity ratio of 39 700 for sample $C1$ predicts for sample $CB1$ the value, 29 000. Since the drift velocity is highly anisotropic, it is probably fortuitous that we find quantitative agreement. In fact, as Cochran and Yaqub have pointed out, many formulas having properties similar to Eq. (42) can be used to correlate resistivity data and mean free paths.

V. FERMI SURFACE

Although considerable information has accumulated over the past few years, our understanding of the band structure and Fermi surface of gallium is far from complete.

The nearly-free-electron (NFE) model, which has given a good first approximation to the electronic bands of many of the simple metals, was shown by Reed and Marcus to be topologically consistent with the galvanomagnetic measurements. Slater, Koster, and Wood,[32] on the other hand, concluded from a study of the free-electron properties of the energy bands that the details of the Fermi surface may be profoundly modified, and de Haas–van Alphen studies by Condon[33] and by Goldstein and Foner,[34] indeed, suggest that this model is not suitable for describing many of the extremal cross sections observed.

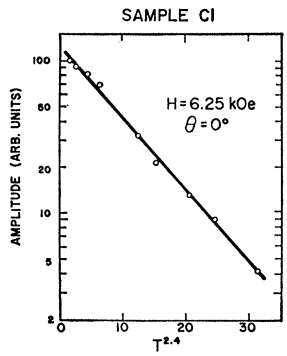

FIG. 15. Temperature dependence of the amplitude of the oscillations in sample $C1$.

Recently, Wood[35] calculated the energy bands for gallium by the augmented-plane-wave (APW) method using a one-electron muffin-tin potential and found, as anticipated, large deviations from the NFE model in all bands, although certain pockets retained a free-electron-like character. There seems to be some support for the modified topology of bands 5 and 6 in this model from the extremal areas determined by the de Haas–van Alphen effect as well as from the radio-frequency size-effect measurements of Fukumoto and Strandberg.[36] Magnetoacoustic experiments, by Bezuglyi, Galkin, and Zhevago[37] on the other hand, have confirmed the exis-

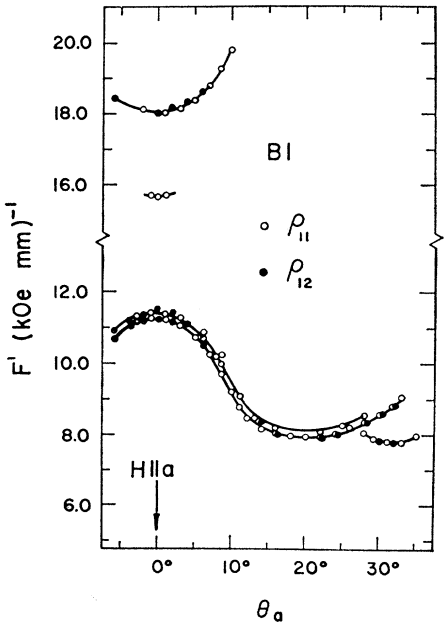

FIG. 14. Reduced frequency plot for sample $B1$ with H in the ac plane.

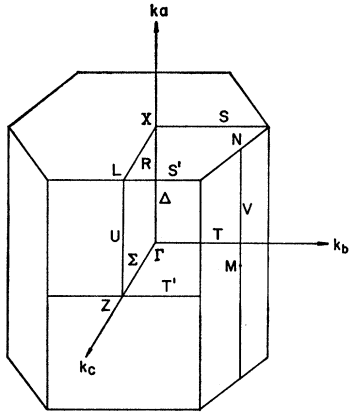

FIG. 16. The Brillouin zone for gallium showing the symmetry points in the notation of Slater, Koster, and Wood.

[32] J. C. Slater, G. F. Koster, and J. H. Wood, Phys. Rev. **126**, 1307 (1962).
[33] J. H. Condon, Bull. Am. Phys. Soc. **9**, 239 (1964).
[34] A. Goldstein and S. Foner, Phys. Rev. **146**, 442 (1966).
[35] J. H. Wood, Phys. Rev. **146**, 432 (1966).
[36] A. Fukumoto and M. W. P. Strandberg, Phys. Rev. **155**, 685 (1967).
[37] P. A. Bezuglyi, A. A. Galkin, and S. E. Zhevago, Zh. Eksperim. i Teor. Fiz. **47**, 825 (1964) [English transl.: Soviet Phys.—JETP **20**, 552 (1965)].

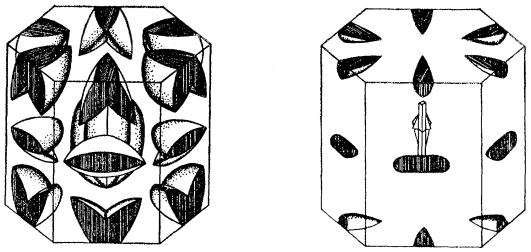

FIG. 17. The 7th- and 8th-band surfaces of the NFE model for gallium as given by Reed and Marcus. The pockets located at the zone edges in the 7th band form the butterflies in the extended zone scheme, and the corresponding sections in band 8, the cigars.

tence of free-electron-like sections in the 7th and 8th bands located at the symmetry point L on the edge of the hexagonal Brillouin-zone face (see Fig. 16). These surfaces, referred to as the "butterfly" and "cigar" (Fig. 17) have been observed also in the de Haas–van Alphen and rf size-effect measurements and seem to follow the NFE model about as well as the APW predictions. Similar pockets at the nonequivalent points N have not been observed experimentally and are probably missing or at least greatly distorted as suggested by the APW calculations.

The orbital area A and derivative $(\partial A/\partial k_z)_{\epsilon_F}$ along the direction of the magnetic field were computed as a function of k_z with H in the $k_a k_b$ plane, the region where the strongest effects were observed. The result of this calculation for a tilt angle of 20° is plotted in Fig. 18. The area in band 8 is maximal for the equatorial orbit, $k_z=0$, and decreases smoothly with k_z. The orbit area at the waist of the butterfly, on the other hand, is minimal, and approaches a maximum just to the left of the saddle point. Consequently, the butterfly gives rise to two distinct sets of oscillations, one of which is degenerate at 0° with the cigar period.

The orbits from which the size-effect oscillations arise are determined by the extremum properties of the derivative $(\partial A/\partial k_z)_{\epsilon_F}$. From Fig. 18(c), the differential area in band 8 vanishes at the waist and drops to an absolute minimum at a small value of k_z. The butterfly also has an extremal orbit which cuts through the surface near the point L for small positive k_z, degenerate with the cigar at 0°. The derivative in this band is discontinuous at the saddle point and has a broad minimum approximately two-thirds of the distance from the point L toward the tip of the lobe, nearly independent of θ. Additional periods of oscillation are possible due to the discontinuity in the derivative at the saddle point which is a limiting point of the hyperbolic type.

TABLE III. Range of the subsidiary periods in the *ab* plane.

	OPW Model	Experimental
F_7	46°–58°	49°–55°
F_{10}	55°–71°	57°–67°
F_{11}	55°–71°	58°–67°
F_{12}	71°–90°	68°–90°
F_{13}	67°–83°	69°–85°
F_{15}	75°–90°	81°–90°
F_{16}	0°–90°	86°–90°

Figure 19 summarizes the main predictions of the NFE model for these bands. The band-8 extremals follow the primary-data periods in the range 0° to 55° remarkably well considering the differential nature of the FS measurements. The frequency associated with the body orbits on the butterfly, on the other hand, is strongly θ-dependent and does not represent the data in this region.

Frequencies F_{10} and F_{11} in Fig. 5 may be identified with the saddle-point orbits in the 7th band in the range 55° to 65°. A more likely explanation, however, is that these frequencies, together with F_7 and F_{13} are associated with limiting point orbits on the cigar and "clamshell" surface which results from magnetic breakdown of the small spin-orbit-induced energy gap at the hexagonal face of the zone. The limiting angles for observing each of these four periods are given in Table III and compare favorably with the ideal angles predicted by the NFE model. The reduced frequency values cannot be estimated since all limiting-point oscillations would have the value 1.45 (kOe mm)$^{-1}$ determined by the Fermi radius independent of θ. The discrepancies are, nevertheless, in the right direction since the influence of neighboring Bragg planes would enhance the Gaussian curvature and, therefore, the characteristic frequency.

The extremal orbits associated with the lobe were observed experimentally only for values of θ near

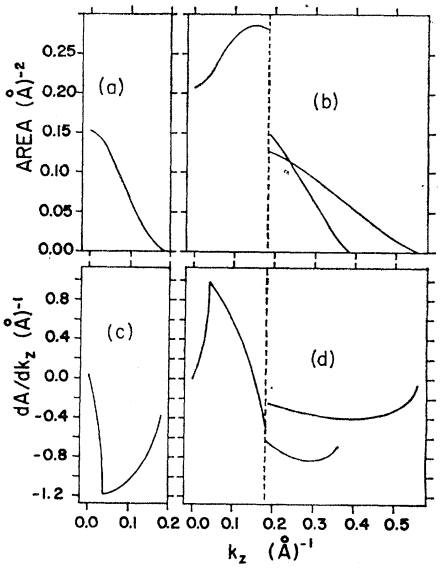

FIG. 18. Orbital area and derivative of the area as a function of k_z from the NFE model. The magnetic field is assumed to be tilted 20° away from the a axis in the ab plane. Curves (a) and (c) refer to band 8, and (b) and (d) to band 7. Due to the inversion symmetry on k space there are other pockets corresponding to bands 8 and 7 which produce dA/dk_z with the same magnitude but opposite sign (see Sec. II).

90° even though the model predicts a large oscillation amplitude for all θ because of the nearly parabolic character of the surface. This is probably due to the relatively slow drift velocity v_z^0 for small θ which makes the phase of the oscillating term in Eq. (32) very sensitive to variations in sample thickness. Under such conditions, neighboring regions in the size-effect specimen would interfere and effectively provide a high-frequency cutoff for the oscillations. These orbits have been observed for H along the a axis in the ultrasonic attenuation[38] with the magnetic field parallel to the sound-propagation direction, and the characteristic frequencies agree to within 10% with the model. For H along b, the lobe orbits in the NFE model yield a reduced frequency $F'=7.3$ (kOe mm)$^{-1}$ and correspond to periods F_{15} and F_{16} in the data. Data frequency F_{14} furthermore, seems to fit the saddle-point orbit 7(c) on the model in this region.

In the APW model where the lobes of the butterfly have shrunk down in size, the surface has been described by Wood as a "cigar with a double pair of wings." Therefore, it is likely that the waist orbits on this surface are modified in such a way that the differential area plot of Fig. 18(d) resembles that for the 8th band, and together would account for two parallel branches near the a axis for the c-type crystals (Fig. 5). A third branch would be attributed to coupling of these orbits through magnetic breakdown across the hexagonal face. Evidence for breakdown of the gap has been found by Goldstein and Foner with H along c in fields of 30 kOe or higher; however, it most likely occurs at much lower magnetic fields in the present case with H in the ab plane for small values of θ since the turning points of the orbits in this geometry are very close to the line LX along which the energy bands are two-fold degenerate. Finally, the APW model suggests the possibility of a fourth parallel branch at the a axis from the band-5 sheet of the Fermi surface which is similar in size and shape to the 7th-band winged cigar.

VI. EFFECT OF MAGNETIC-FIELD ORIENTATION, SAMPLE SIZE, AND SURFACE PREPARATION ON THE OSCILLATORY AMPLITUDES

For all size effects a coherent discontinuity in the motion of the current carriers is required. This coherence is supplied by the precise parallelism and smoothness of the two opposing sample surfaces. Diffuse scattering of the electrons is required to give a definite cutoff to the path integral in Eq. (5). That is, a collision with the surface which interrupts the transverse (to ζ) oscillatory motion of the electron must occur in a layer which is thin compared with the distance travelled in a cyclotron oscillation. In this section we discuss and qualitatively improve some of the approximations of Sec. II which affect these considerations.

First we calculate the influence of the rectangular cross section on closed orbits. From Fig. 1 we see, upon considering the electrons moving along H, that only those terminating at the upper surface along the length $d_\zeta - d_\xi \tan\theta$ are effective[20] in contributing to $\Delta\sigma$. In addition there are contributions to σ^0 from the electrons originating on the left face and terminating on the upper surface along the length $d_\xi \tan\theta$ as well as from those originating at the bottom surface along the length $d_\xi \tan\theta$ and terminating on the right face. These considerations[16] and Eqs. (15) and (16) yield

$$\Delta\sigma_{ij}=[1-(d_\zeta/d_\xi)\tan\theta]\Delta\sigma_{ij}(d_\zeta), \tag{43}$$

$$\sigma_{ij}^0=[1-(d_\zeta/d_\xi)\tan\theta]\sigma_{ij}^0(d_\zeta) + 2\sec\theta/(d_\xi d_\zeta)\int_0^{d_\zeta \sin\theta} dx\,\sigma_{ij}^0(x\csc\theta)\,x\csc\theta. \tag{44}$$

Evaluation of the integral in Eq. (44) yields

$$\sigma_{ij}=\frac{4e^2}{h^2}\int_{v_\zeta^0>0} dk_z m^* \tau v_i^0 v_j^0\left[1-v_\zeta^0\tau\left\{\frac{1}{d_\zeta}+\frac{\tan\theta}{d_\xi}\left(1-2\frac{v_\zeta^0\tau}{d_\zeta}\right)-\left[\frac{1}{d_\zeta}-\frac{\tan\theta}{d_\xi}\left(1+2\frac{v_\zeta^0\tau}{d_\zeta}\right)\right]\exp(-d_\zeta/v_\zeta^0\tau)\right\}\right]$$
$$+\frac{8e^2}{h^2}\int_{v_\zeta^0>0} dk_z m^*\tau\sum_{n\geq 1}\left\{\left[1-v_\zeta^0\tau\left(\frac{1}{d_\zeta}+\frac{\tan\theta}{d_\xi}\right)\frac{1-(n\omega_c\tau)^2}{1+(n\omega_c\tau)^2}\right]\frac{\mathrm{Re}(v_i^{(-n)}v_j^{(n)})}{1+(n\omega_c\tau)^2}\right.$$
$$\left.+\left[1-v_\zeta^0\tau\left(\frac{1}{d_\zeta}+\frac{\tan\theta}{d_\xi}\right)\frac{2n\omega_c\tau}{1+(n\omega_c\tau)^2}\right]\frac{n\omega_c\tau\,\mathrm{Im}(v_i^{(-n)}v_j^{(n)})}{1+(n\omega_c\tau)^2}\right\}, \tag{45}$$

which for long mean free path and large magnetic field ($l\gg d_\zeta$ and $\omega_c\tau\gg 1$) becomes

$$\sigma_{ij}^0\approx\frac{2e^2 d_\zeta}{h^2}\int_{v_\zeta^0>0} dk_z\frac{v_i^0 v_j^0}{v_\zeta^0}\left[1-\frac{1}{3}\frac{d_\zeta}{v_\zeta^0\tau}-\frac{1}{3}\frac{d_\zeta}{d_\xi}\tan\theta\left(1-\frac{1}{2}\frac{d_\zeta}{v_\zeta^0\tau}\right)\right]$$
$$+\frac{8}{d_\zeta}\left(\frac{c}{hH}\right)^2\int_{v_\zeta^0>0} dk_z (m^*)^3 v_\zeta^0\left\{\left[1+\frac{d_\zeta}{d_\xi}\tan\theta+\frac{d_\zeta}{v_\zeta^0\tau}\right]\sum_{n\geq 1} n^{-2}\,\mathrm{Re}(v_i^{(-n)}v_j^{(n)})\right.$$
$$\left.-2\left[1+\frac{d_\zeta}{d_\xi}\tan\theta\right]\sum_{n\geq 1} n^{-2}\,\mathrm{Im}(v_i^{(-n)}v_j^{(n)})\right\}+\frac{8ec}{h^2 H}\int_{v_\zeta^0>0} dk_z (m^*)^2\sum_{n\geq 1}[1-1/(n\omega_c\tau)^2]n^{-1}\,\mathrm{Im}(v_i^{(-n)}v_j^{(n)}). \tag{46}$$

[38] J. A. Munarin, Bull. Am. Phys. Soc. 12, 332 (1967).

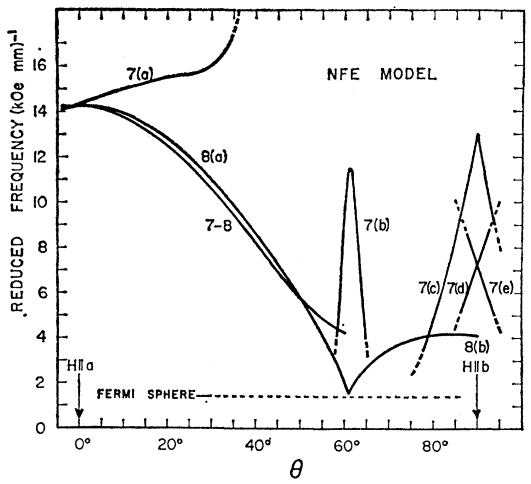

FIG. 19. Reduced frequency predicted by the NFE model for the butterfly and cigar surfaces located at L.

Equation (46) shows that for a sample with small cross section the bulk conductivity is transformed into a form which no longer is directly proportional to the relaxation time or mean free path.

Reed and Marcus showed from their measurements that the sixth-band "hole" FS has the topology of a cylinder whose axis is parallel to the k_c direction and is the only surface capable of producing open orbits.[21] For open orbits there are two components of the drift velocity. In Eq. (19) we have already given the expression for v_a^0. The drift along the b axis is

$$v_b^0 = \cos\theta\ \hbar K_c/2\pi m^* + \sin\theta\ v_z^0 \qquad (47)$$

for H in the ab plane. Thus, the open orbits can connect (α) the parallel faces whose normal is parallel to the ξ axis, as well as (β) the adjacent faces, and (γ) the opposite faces whose normal is parallel to the ζ axis (those connected by closed orbits). For a particular open orbit (α) prevails when $|v_\xi^0/v_\zeta^0| > d_\xi/d_\zeta$; the reverse inequality produces (γ). When $\mathbf{H}$ is exactly along the a axis, there is only a very thin band (Δk_z) of the FS supporting open orbits (producing drift motion in real space along the ξ axis); these orbits are slightly elevated from the central section and have considerable drift velocity v_ζ^0 with only a small oscillatory motion along the a axis (see Ref. 21, Figs. 14 and 15). When $\mathbf{H}$ is rotated toward the b axis, however, there exist open orbits with $v_\zeta^0 = 0$ whose oscillations $v_\zeta^{\rm osc}$ cause the "holes" to move up and down from the sample surface to a repeatable depth while they are drifting along the ξ axis. [Setting Eq. (19) to zero and plugging into Eq. (47) shows, in this case, $v_b^0 = \hbar K_y/(2\pi m^*)$, as expected.] This motion produces current splashes under the vacuum-metal interface at depths $\zeta \approx v_\zeta^{\rm osc}/\omega_c$ in the metal. Such orbits are of class (α) and have very complicated structure because of the many turning points within the interval K_c (see Ref. 21, Figs. 14 and 15). The current splashes arise from the places where $v_\zeta = 0$; they are very short in length due to the small radius of curvature at these points.

The oscillations in the voltage which we observe in the experiment are due to the motion of the electrons back and fourth in the dc current flowing in the sample. For each completed motion (per cyclotron period) there is no net energy absorbed by the electron (for long mean free paths). The time of interaction of the electron with the ith component of the dc current is determined by the average radius of curvature on those portions of the orbit contributing to the v_i. In Sec. V we have identified many of the periods discussed in Sec. IV with the 7th- and 8th-band electron FS located at the symmetry point L in the Brillouin zone (see Fig. 16). Keeping in mind that the velocity is determined by the normal to the FS, an examination of Fig. 17 shows that the radius of curvature associated with v_b is large, while v_c is associated with small radius of curvature. Therefore $\Delta\sigma_{xx}$ will be unaffected by the current splashes, while $\Delta\sigma_{xy}$ and $\Delta\sigma_{zy}$ will be diminished considerably due to interference from these open-orbit current splashes. We associate the rapid diminution of oscillatory Hall voltage for c-type samples when $\theta_a > 2^0$ with this effect. Mathematically, the inclusion of the skimming orbit current sheets necessitates the elimination of $E_\zeta(\zeta)$ in terms of the homogeneous E_ξ and E_y [39]; this step (not included in Sec. II) links an orbit from one piece of FS with the (self-consistent) electric field due to orbits on another piece. For b-type samples a rotation of $\mathbf{H}$ toward the c axis transforms open orbits into closed ones; the only drift motion for closed orbits is along $\mathbf{H}$; this drift motion moves the current carriers into the depths of the sample. Therefore, no current splashes are produced by these orbits in a dc experiment.[39]

One expects that class (α) open orbits would contribute signals to the voltage oscillations we observe. However, no frequencies were observed in our ($CB1$, $CA1$, $C1$)-comparison experiments which would require d_ξ rather than d_ζ for data reduction. From the theory of Sec. II we see that for most of the orientations of $\mathbf{H}$ in the ab-plane open orbits must not have been excited. (The high-field growth in the resistivity oscillations are due to finite radii orbits in a compensated metal where $\sigma_{xx}^0 \sim 1/H^2$.) When $\mathbf{H}$ was within 5° of the b axis, the amplitude of the oscillations was not only reduced 50 times but exhibited a decay rather than growth with $\mathbf{H}$. These facts are consistent with expectations since in practice it proves impossible to keep exciting open orbits as $\mathbf{H}$ is rotated in the ab plane.[21] When $\mathbf{H}$ is not near the b axis, a slight misorientation converts the open orbits into extended ones which do not reach all the way across the sample. The extent of the trajectory in real space when $\mathbf{H}$ is misaligned by a small angle $\delta\theta$ is

[39] M. Ya. Azbel and V. G. Peschanskii, Zh. Eksperim. i Teor. Fiz. 49, 572 (1965) [English transl.: Soviet Phys.—JETP 22, 399 (1966)].

given by[40]

$$d_{\text{ext}} \leq (\delta k_\zeta)\hbar c/(eH\,\delta\theta), \tag{48}$$

where δk_ζ is the size of the open-surface neck joining one Brillouin zone to the next. For **H** along the b axis[41] $\delta k_\zeta \approx 0.39\times 10^8$ cm^{-1} and $d_{\text{ext}} < 1$ mm for $H \gtrsim 5$ kOe and $\delta\theta > 3°$. However, for **H** near the a axis[21] $\delta k_\zeta \approx 0.03\times 10^8$ cm^{-1} and $d_{\text{ext}} < 1$ mm for $H \gtrsim 5$ kOe and $\delta\theta > \frac{1}{4}°$. The extended orbits would still produce the current splashes as described above, but would change the det σ^0 from the open-orbit dependence H^{-2} to the compensated dependence, H^{-4}. The nonappearance of class (α) frequencies when **H** is near the b axis and open orbits are excited may be attributed to the complicated motion described above; it would give rise to high-frequency oscillations which would be unobservable due to their sensitivity to any surface irregularities. (See also the discussion in Sec. V.) Pippard[42] recently considered the amplitude dependence of the conductivity oscillations from a two-dimensional open orbit and found the H^{-2} behavior which we see from Eq. (16) is just a consequence of the two-dimensionality (dropping the k_z integration) and not the openness.

The amplitude dependence exhibited in Fig. 6 can be qualitatively explained in the light of the discussion given here and in Sec. II. The sharp rise in $F6$ in the vicinity of 15° is probably due to signals from the saddle point on the butterfly as discussed in Sec. V; this behavior is very much like the description of Sec. II [Eq. (28)]. Otherwise the trend is a slow fall in amplitude up to about 30° and then a rapid one to zero at the body diagonal. Since $|\partial A/\partial k_z|$ is increasing to 26° (Fig. 10) and secθ is increasing, this behavior may be understood from Eqs. (23) and (43) as a balance between the increase expected from the $(dA/dk_z)^4$ factor and the decrease expected from the secθ-dependent factors. A complete understanding of the angular dependence of the amplitude would require a Fourier analysis over a much smaller field region so that the amplitude of each component versus the (average) field strength can be determined. Then a calculation of (modified) orthogonalized-plane-wave (OPW) $(\partial A/\partial k_z)$ and higher derivatives (where required for the formulas of Sec. II) versus H orientation would have to be compared with the data.

As $H \to \infty$ the compensated metal becomes transformed into an uncompensated one due to the growth of the small-coefficient H-dependent term in D of Eq. (38). However, before the onset of this "saturation" the effect of surface imperfections becomes important. First we note from Eq. (2) that a discrepancy in the thickness of the sample shifts the phase of the observed oscillations. For example, a modification of 0.0001 in.

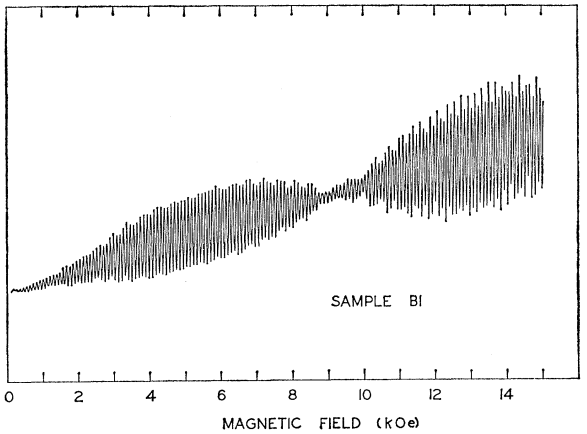

FIG. 20. First derivative of magnetoresistivity for sample BA-II (Ref. 10) for H 7.4° from a axis in ac plane. Note that the maximum amplitude for this specimen (which was sandblasted) occurs at approximately 6 kOe. The de Haas–Schubnikov oscillations are seen above 10.5 kOe. The size-effect oscillations are not seen with noticeable strength above 10.5 kOe.

in a 1-mm sample causes a phase shift of 10.5° at 1 kOe. This makes evident the necessity of careful surface preparation. If the sample surface is perfectly smooth and free of stresses, one might worry about the effect of the specular scattering of electrons. If the electron-cyclotron radius is large compared with surface imperfections, it sees a flatter surface and the probability of specular scattering is larger. As the magnetic field strength is increased and the cyclotron radius becomes comparable and less than the extent of surface blotches the specularity would tend to disappear. However, in metals, small-angle scattering processes are important and in most practical cases there is a smearing out of the specularity. Specular scattering of the electrons at the metal-vacuum boundary implies conservation of the momentum parallel to the interface. In general this does not imply continuity of the transverse velocity; thus in our case this is equivalent to diffuse scattering.[43,44] For a nonspherical FS (unless the FS is a closed surface of revolution about the H direction) in-valley specular scattering (staying within the same band) does not conserve transverse velocity. Only if there is a special relationship of the z axis (H direction), ζ axis (normal to sample surface), and the crystal lattice so that the reflection of the electron across the Brillouin zone (intervalley scattering) under specular scattering (conservation of transverse momentum and reversal of p_ζ) means a continuity in $m^* v_\zeta{}^0$ and transverse velocity, will the amplitude of the resistivity oscillations be diminished [because of the unsharp cutoff of the path integral of Eq. (5)]. When the Sondheimer oscillations (limiting-point electrons with infinitesimal radii) are being observed from a FS of revolution with H parallel

[40] I. M. Lifshitz and V. G. Peschanskii, Zh. Eksperim. i Teor. Fiz. **35**, 1251 (1958) [English transl.: Soviet Phys.—JETP 8, 875 (1959)].
[41] J. A. Munarin and Y. Eckstein, Phys. Rev. Letters, **19**, 1426 (1967).
[42] A. B. Pippard, Phil. Mag. **13**, 1143 (1966).
[43] We are thankful to R. F. Greene for discussing these points (private communication).
[44] R. F. Greene, Phys. Rev. **141**, 687; **141**, 690 (1966).

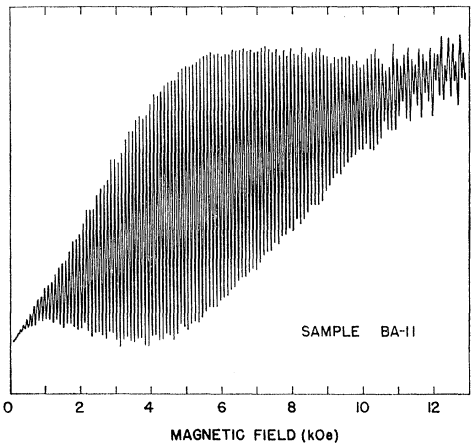

FIG. 21. First derivative of magnetoresistivity for sample $B1$ for H in same approximate orientation as Fig. 20. This sample was not sand-blasted. After a node at 9 kOe the size-effect oscillations continue growing in amplitude to largest fields.

to the ζ axis,[8] the effects of specualr scattering will probably be negligible since the specularity is least for those electrons moving straight at the boundary.

In most of our experiments the amplitude of the oscillations continued to increase out to the highest fields (16 kOe). Foner and McNiff[11] (1967) have observed the increase in the amplitude of the oscillations out to 42 kOe followed by a continuous decrease to their highest fields (95 kOe). We reexamined some data previously taken from b-type samples which had their surfaces sandblasted with particles 23 μ in diam. See Figs. 7 and 20. We notice that curves $B1$ and $B2$ in Fig. 7 show exactly the same behavior (except occurring in the range 4 to 12 kOe) as that shown in Foner and McNiff's Fig. 2 (1967).[11] It is interesting to note that as H increases both the cyclotron diameter and the distance travelled by the electron during one cyclotron period, $2\pi v_\zeta{}^0/\omega_c = (\mathrm{F'H})^{-1}$ [from Eqs. (2) and (40)], become comparable to 23 μ in the range 5 to 7 kOe. For larger fields the surface irregularities incoherently scatter the electrons and reduce the oscillation amplitudes. In Fig. 21 we show for comparison the magnetoresistivity oscillations for a b-type sample with a "smooth" surface. Its amplitude is still growing out to our highest fields.

VII. SUMMARY

These results clearly establish that size-dependent oscillations in the transport properties occur for regions of the Fermi surface where $(\partial A/\partial k_z)_{\epsilon_F}$ has an extremum, as well as for those which contain elliptical limiting points. In this case, however, the amplitude dependence in the high-field limit may be considerably modified according to the nature of the singularity and can be correctly established only by taking into account the dependence on magnetic field of the entire conductivity tensor (compensated, with open-orbit contributions, or uncompensated), the boundary scattering of the resonant electrons by the surface imperfections, and open-orbit current sheets. The size-dependent oscillations in gallium have been studied in detail, and the main branches correspond quite well to the theory and seem to arise from orbits in the 7th-, 8th-, and possibly 5th-band sheets of the Fermi surface. An improved model will be needed to establish this relationship unequivocally since the differential nature of the effect is sensitive to small distortions in the geometry. Similar oscillatory effects are expected to occur in the lens-shaped band surface of the divalent hexagonal metals as well as in their butterflies.[45]

ACKNOWLEDGMENTS

The authors take pleasure in acknowledging a number of helpful discussions on various aspects of the problem with J. H. Condon, J. E. Graebner, J. B. Ketterson, S. G. Eckstein, Y. Eckstein, P. Hambourger, and R. F. Greene.

[45] Recently, size-effect oscillations similar to those observed here have been reported in cadmium and are attributed to a broad minimum in dA/dk_z in the radial direction in the 3rd-band lens. See P. D. Hambourger, J. A. Marcus, and J. A. Munarin, Phys. Letters **25A**, 461 (1967).